# Alteration minerals, uids, and gases on early Mars: Predictions from 1-D ow geochemical modeling of mineral assemblages in meteorite ALH 84001

The Meteoritical Society

*Meteoritics & Planetary Science* 51, Nr 11, 2154–2174 (2016)
doi: 10.1111/maps.12713

# Alteration minerals, fluids, and gases on early Mars: Predictions from 1-D flow geochemical modeling of mineral assemblages in meteorite ALH 84001

Mohit MELWANI DASWANI[1,2,*], Susanne P. SCHWENZER[3], Mark H. REED[4], Ian P. WRIGHT[1], and Monica M. GRADY[1]

[1]Department of Physical Sciences, The Open University, Walton Hall, Milton Keynes MK7 6AA, UK
[2]Department of the Geophysical Sciences, University of Chicago, 5734 S. Ellis Ave., Chicago, Illinois 60637, USA
[3]Department of Environment, Earth and Ecosystems, The Open University, Walton Hall, Milton Keynes MK7 6AA, UK
[4]Department of Geological Sciences, University of Oregon, Eugene, Oregon 97403, USA
[*]Corresponding author. E-mail: melwani@uchicago.edu

*(Received 23 October 2015; revision accepted 16 June 2016)*

**Abstract**–Clay minerals, although ubiquitous on the ancient terrains of Mars, have not been observed in Martian meteorite Allan Hills (ALH) 84001, which is an orthopyroxenite sample of the early Martian crust with a secondary carbonate assemblage. We used a low-temperature (20 °C) one-dimensional (1-D) transport thermochemical model to investigate the possible aqueous alteration processes that produced the carbonate assemblage of ALH 84001 while avoiding the coprecipitation of clay minerals. We found that the carbonate in ALH 84001 could have been produced in a process, whereby a low-temperature (~20 °C) fluid, initially equilibrated with the early Martian atmosphere, moved through surficial clay mineral and silica-rich layers, percolated through the parent rock of the meteorite, and precipitated carbonates (thereby decreasing the partial pressure of $CO_2$) as it evaporated. This finding requires that before encountering the unweathered orthopyroxenite host of ALH 84001, the fluid permeated rock that became weathered during the process. We were able to predict the composition of the clay minerals formed during weathering, which included the dioctahedral smectite nontronite, kaolinite, and chlorite, all of which have been previously detected on Mars. We also calculated host rock replacement in local equilibrium conditions by the hydrated silicate talc, which is typically considered to be a higher temperature hydrothermal phase on Earth, but may have been a common constituent in the formation of Martian soils through pervasive aqueous alteration. Finally, goethite and magnetite were also found to precipitate in the secondary alteration assemblage, the latter associated with the generation of $H_2$. Apparently, despite the limited water–rock interaction that must have led to the formation of the carbonates ~ 3.9 Ga ago, in the vicinity of the ALH 84001 source rocks, clay formation would have been widespread.

## INTRODUCTION

In the wake of the *Curiosity* rover's discovery (Farley et al. 2014; Vaniman et al. 2014) of smectites in ~4.21 Ga old crater-rim derived rocks in >3.5 Ga (Thomson et al. 2011; Deit et al. 2013) Gale crater on Mars, the absence of secondary phyllosilicates in the ancient (~4.1 Ga) Martian meteorite ALH 84001 requires further investigation. If clay minerals are ubiquitous on the ancient terrains of Mars and the secondary carbonates in the meteorite are formed by low-temperature aqueous alteration of the host rock, why are there no secondary phyllosilicates in ALH 84001 formed by this process?

Clay minerals were predicted to occur on the surface of Mars as a result of aqueous alteration of the basalts (e.g., Zolensky et al. 1988) and have been detected since, both from orbital hyperspectral spectrometers (e.g., Bibring et al. 2006; Mustard et al. 2008) and in situ with the instruments on the NASA rover MSL *Curiosity* (Vaniman et al. 2014), and probably *Opportunity* (e.g., Arvidson et al. 2014).

Within the Mawrth Vallis region and in Nili Fossae (both of Noachian-age, >3.7 Ga), Fe/Mg-bearing smectites and Al-rich clays have been interpreted as the results of weathering at "moderate to alkaline pH" (Mustard et al. 2008). On the other hand, $Fe^{3+}$-rich smectites at Matijevic Hill, at the rim of Endurance Crater (also Noachian in age) are interpreted as having been formed by the neutralization of fluids that were originally "mildly acidic" in character, with pH > 5 (Arvidson et al. 2014).

Carbonates have also been detected by orbital spectroscopy at Nili Fossae outcrops and possibly in dust (see reviews by Ehlmann and Edwards [2014] and Niles et al. [2013]). In situ, they have been detected in soil by the *Phoenix* lander (Boynton et al. 2009), and by the *Spirit* rover in an outcrop at the Columbia Hills in Gusev crater (Morris et al. 2010). But the large, widespread outcrops of carbonates predicted by models of a warm early Martian climate (e.g., Fanale et al. 1982; Pollack et al. 1987) have failed to materialize: compared to the clay minerals, carbonates are rare and highly localized. However, a recent reanalysis of orbital data points to somewhat more extensive occurrences of carbonates on the surface of Mars, together with a spatial (and possibly chemical) relationship with clay minerals (Wray et al. 2016).

Here we aim to constrain the pH and composition of the carbonate and clay mineral-forming fluids of the ancient terrain where ALH 84001 was emplaced.

## Aqueous Alteration in 84001

The ~4.1 Ga old (Lapen et al. 2010) meteorite ALH 84001 is the only known Martian meteorite entirely belonging to the Noachian near-surface of Mars. It is composed of ~97% orthopyroxene ($En_{70}Wo_3$), ~1% chromite, and ~1% maskelynite ($An_{31}Ab_{63}$) by volume; abd minor amounts of phosphates (mainly apatite), olivine ($Fo_{65}$), augite ($En_{45}Wo_{43}$), and silica glass (Mittlefehldt 1994; Treiman 1995, 1998; Shearer et al. 1999). A ~3.92 Ga (Nyquist et al. 2001) zoned carbonate secondary assemblage in ALH 84001 forms ~1 vol% of the meteorite (Mittlefehldt 1994). It occurs in interstices and replacing maskelynite and orthopyroxene (Mittlefehldt 1994; Treiman 1995; Kring et al. 1998) and can be divided into at least two distinct groups: "rosette"-type spheroid-zoned concretions, and massive ankeritic "slab"-like domains (Eiler et al. 2002b; Corrigan and Harvey 2004). Most rosettes measure ~50 to 200 μm in diameter and are composed of orange-colored cores of ankerite–magnesiosiderite/ankerite–dolomite solid solution or ferromagnesian calcite, overlain by a ~5–10 μm thick black rim of siderite (with substantial admixed nanocrystalline magnetite), itself coated by a ~10–15 μm white magnesite rim and another black siderite–magnetite rim (e.g., McKay et al. 1996; Eiler et al. 2002b; Thomas-Keprta et al. 2009). (A ternary diagram of representative carbonate compositions is shown in Fig. 1a.) Sulfide grains (pyrite, and possibly pyrrhotite and greigite) occur next to primary chromite grains and within the carbonates, with some apparently in carbonate-crossing veins (Mittlefehldt 1994; Treiman 1995; McKay et al. 1996; Greenwood et al. 2000; Eiler et al. 2002b; Thomas-Keprta et al. 2009). Trace amounts of apparently preterrestrial fine-scaled phyllosilicates ("phlogopitic mica") intergrown with the carbonates have been described, possibly postdating the carbonate deposition (Brearley 2000).

Magnetite nanocrystals, together with polycyclic aromatic hydrocarbons, sulfides, and fossil-like structures within the carbonate rosettes were interpreted as possibly biogenic (e.g., McKay et al. 1996; Thomas-Keprta et al. 2000), but an abiotic origin for these has since been explained (e.g., Golden et al. 2000, 2001; Steele et al. 2007; Treiman and Essene 2011). A large range of pressure–temperature (P-T) conditions have been invoked to explain the abiotic formation of the alteration assemblage (see supporting information, Fig. S1). But stable isotope analyses have shown that relatively low-temperature fluids were responsible for producing the carbonates. Specifically, the higher $\delta^{18}O_{SMOW}$ in the carbonates compared to the host rock is indicative of an external source for the carbonates, particularly from a permeating fluid (Romanek et al. 1994). The large range in high $\delta^{18}O$ (0–+22.6 ‰; Romanek et al. 1994; Valley et al. 1997; Eiler et al. 2002a) and $\delta^{13}C_{PDB}$ (+27–+64 ‰; Grady et al. 1994; Romanek et al. 1994; Jull et al. 1997; Niles et al. 2005; Valley et al. 1997; Niles et al. 2005; Halevy et al. 2011) suggests high variability of $\delta^{18}O$ and $\delta^{13}C$ within the carbonates themselves, and that the carbonates did not experience equilibrium with the host rock or compositional and isotopic homogenization, as would occur at high temperatures (e.g., Hoefs 2009, p. 15) typical in metamorphic carbonates (e.g., Sheppard and Schwarcz 1970). A precise temperature of 14–22 °C for the formation of the carbonates was determined by C-O clumped isotope thermometry (Halevy et al. 2011). The mechanism favored by most investigators for the low-temperature formation of the zoned carbonate is evaporation (McSween and Harvey 1998; Warren 1998), whereby in a short time scale, flood waters percolated through ALH 84001 and precipitated the carbonates while the water evaporated, resulting in the compositional and isotopic zonation observed in them, and accounting for the lack of other secondary

minerals. Other authors expanded the evaporitic scenario (e.g., Scott 1999; Eiler et al. 2002a; Knauth et al. 2003; Holland et al. 2005; Niles et al. 2009; Halevy et al. 2011). Furthermore, rubidium and strontium systematics in ALH 84001 point to pre-existing phyllosilicates as the origin of $^{87}Rb/^{86}Sr$ enrichment in the carbonates, suggesting that fluids leached phyllosilicates prior to forming the carbonates (Beard et al. 2013).

The apparent paradox between the presence of carbonates but the absence of clays in the meteorite, and the presence of phyllosilicates but the rarity of carbonates on the surface of early Mars, can be addressed as a multicomponent mineral–liquid–gas system that can be simulated with thermochemical modeling. The pressure–temperature (P-T) conditions related to a suite of geological contexts can be used in the software to simultaneously assess the relative stabilities of large sets of observed and predicted mineral phases that would occur in natural systems. Conversely, the presence of a particular set of alteration minerals which are computed to be stable in a modeled system is indicative of specific P-T conditions which can be extended to describe a natural system and infer geological processes where the calculated alteration minerals are present.

## THERMOCHEMICAL MODELING METHOD

### Mineral Precipitation and Equilibria Computations

We used the thermochemical modeling software CHIM-XPT (Reed 1998) to simulate aqueous alteration of the ALH 84001 host rock. The program uses a modified Newton–Raphson method to solve equations of chemical equilibria for aqueous species and minerals in its database using extended Debye–Hückel theory from Tanger and Helgeson (1988) (Reed 1982, 1998; Spycher and Reed 1988). The database is derived and modified from the updated SUPCRT92/SUPCRT 2007 databases (Johnson et al. 1992) available at http://geopig.asu.edu/sites/default/files/slop07.dat, and mineral, gas, and heat capacity data from Holland and Powell (2011). (Further details on the database can be found at http://pages.uoregon.edu/palandri/.) CHIM-XPT and its predecessor, CHILLER, have been used to characterize phyllosilicate compositions at impact-generated hydrothermal systems on Mars (Bridges and Schwenzer 2012; Filiberto and Schwenzer 2013; Schwenzer and Kring 2013), low-temperature (13 °C) aqueous alteration conditions postdating hydrothermal activity at a Noachian-aged impact site (Filiberto and Schwenzer 2013), clay minerals forming the Sheepbed mudstones at Yellowknife Bay in Gale Crater (Bridges et al. 2015), and the fluids associated with the clay formation (Schwenzer et al. 2016).

All our models were run at 20 °C, which is comparable with the estimate of the temperature at which the carbonates may have precipitated in the meteorite according to C-O clumped isotope thermometry (Halevy et al. 2011), but is significantly higher than average Martian surface temperatures at present. We disallowed the formation of dolomite and other minerals whose growth is kinetically retarded under these low-temperature conditions (e.g., Arvidson and Mackenzie (1999), and see supporting information (Table S1) for more references and all disallowed minerals. Magnesite, e.g., was actively suppressed as it is kinetically retarded (e.g., Hänchen et al. 2008), though the Mg-bearing carbonates, huntite ($Mg_3Ca(CO_3)_4$) and nesquehonite ($MgCO_3 \cdot 3H_2O$), were allowed to form. Both huntite and nesquehonite can serve as precursors to magnesite. The latter rapidly transforms to hydromagnesite ($(Mg_5(CO_3)_4(OH)_2 \cdot 4H_2O$) by the loss of crystalline water and dehydroxylation with a minor temperature increase (≥52 °C; Davies and Bubela 1973) and then to magnesite at >220 °C (Hollingbery and Hull 2010), consistent with the observation of higher P-T magnetite and graphite in the meteorite (Treiman and Essene 2011; Steele et al. 2012b). Methane ($CH_4$) equilibration and formation with the reduction of $H_2O$ and $CO_2$ was also prohibited in the models, given the kinetic barrier to abiogenic $CH_4$ formation at low temperature (e.g., Seewald et al. 2006; McCollom 2013).

CHIM-XPT is able to calculate the molar fraction of endmember minerals for a number of ideal solid solution minerals. Minerals that form solid solutions and that precipitated in the models are grouped in the results for clarity, e.g., "chlorite" in the figures includes the solid solution endmembers clinochlore ($Mg_5Al_2Si_3O_{10}(OH)_8$), chamosite ($Fe_5Al_2Si_3O_{10}(OH)_8$), penantite ($Mn_5Al_2Si_3O_{10}(OH)_8$), and "Al-free chlorite" ($Mg_6Si_4O_{10}(OH)_8$). Carbonate compositions, on the other hand, are addressed in the results as compositional mixtures of computed discrete mineral phases, as CHIM-XPT does not calculate carbonate solid solutions, e.g., ankerite ($(CaFe)(CO_3)_2$) is different to calcite ($CaCO_3$) + siderite ($FeCO_3$), although compositionally identical. We allowed a continuous range of carbonate compositions to form between the carbonate mineral endmembers, but assumed that intermediate compositions form as a result of mixing between the precipitating endmembers. We report the saturation indices of carbonate minerals in the supporting information (Fig. S2) to address this

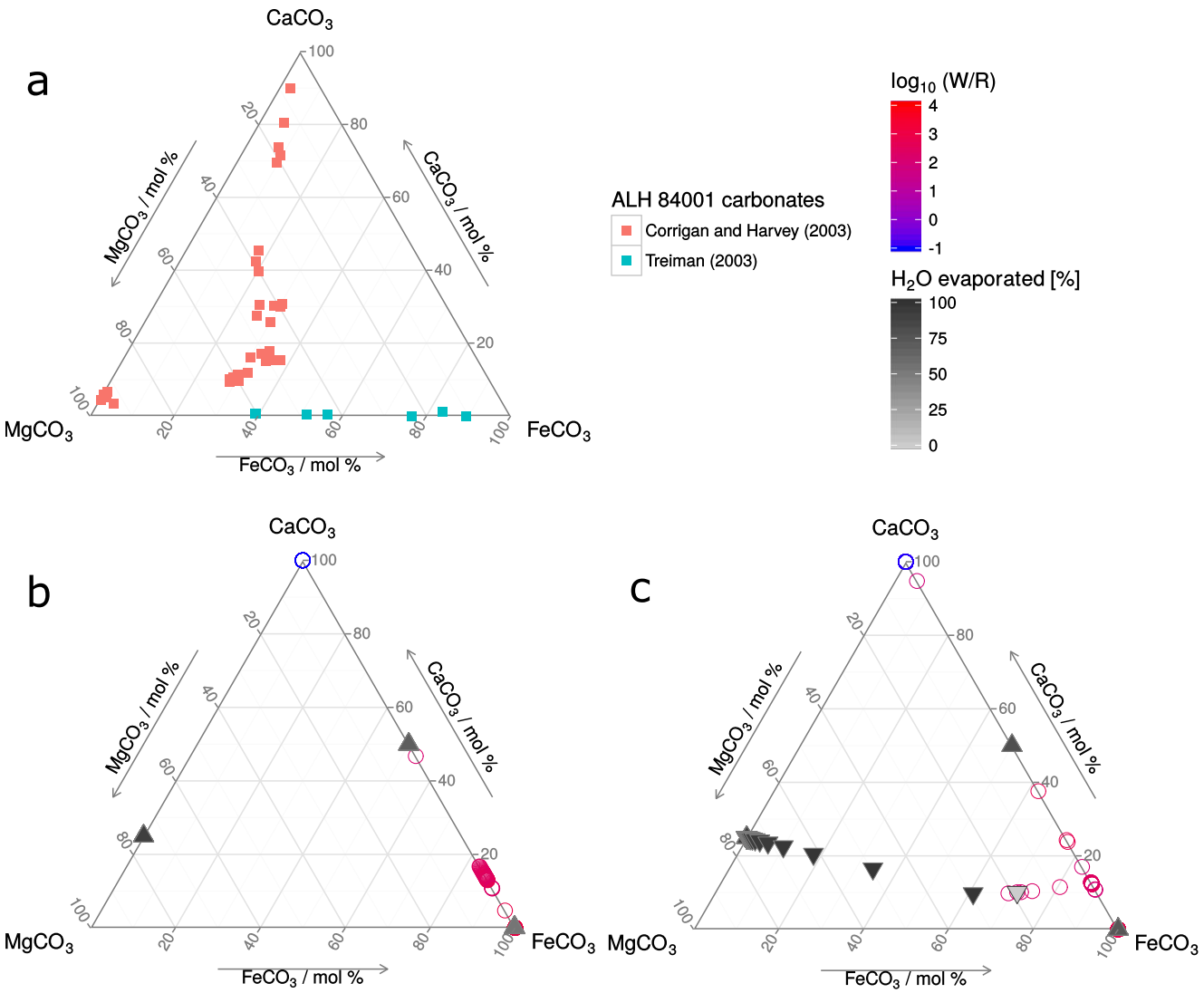


Fig. 1. Carbonate composition ternary diagrams of (a) representative metastable carbonate compositions in ALH 84001 reported by Corrigan and Harvey (2004) and Treiman (2003); (b) carbonate compositions formed in *Model A* (initial $fCO_2$ = 0.5 bar); (c) carbonate compositions formed in *Model B* (initial $fCO_2$ = 1 bar). Circles in (b) and (c) represent carbonate compositions precipitated in the 1-D flow models at different water to rock (W/R) ratios. Upright triangles show compositions precipitated as a function of water evaporated at $\log_{10}$ W/R = 3, and triangles pointing down are the same but at $\log_{10}$ W/R = 2. Evaporations at $\log_{10}$ W/R = 1 and $\log_{10}$ W/R = 0 only precipitated $CaCO_3$, and are not shown here (see Table 3).

shortcoming, and point out that this method allows us to put upper limits on the cations and $CO_3^{2-}$ in solution required to form the carbonates, as multiple carbonate endmembers (e.g., huntite and calcite) must both saturate and precipitate to form intermediate compositions (e.g., magnesian calcite). Further solid solutions and mineral endmembers are detailed in the supporting information (Table S2).

We did not seek to simulate the morphology of the carbonate rosettes, but aimed to understand the conditions at which the diverse carbonate compositions precipitated, the compositions of the associated alteration fluid, and the precipitation and stability of other secondary phases which may or may not be relevant to the carbonate minerals in ALH 84001. We regard a model as an instructive possibility when the resulting mineral assemblage resembles the compositional range of the carbonates in ALH 84001, while minerals other than carbonates are absent or minor.

## Starting Conditions

Table 1 lists the starting conditions of each model computed here. The composition of the initial rock used in the alteration models was an "unaltered" ALH 84001, i.e., the host rock mineralogy of ALH 84001 minus the carbonate minerals, and assuming olivine and other minerals were not present prior to alteration (Table 2). All rocks and minerals are specified in our thermodynamic database as sums of elemental molar abundances, i.e., our models make no provision for differential solubilities or reaction rates of the constituent minerals, but nevertheless, ~99 wt% of the host is orthopyroxene. Ti and Cr compounds were not included as reactants because the database does not include Ti and Cr species and minerals. Given the relative insolubility of Ti(IV) and Cr(III) oxides in natural waters under ambient conditions (e.g., Imahashi and Takamatsu 1976; Richard and Bourg 1991), and their low abundance in ALH 84001 (principally in accessory chromite), we consider that their importance on secondary mineral composition and chemical speciation of solutes was negligible.

Table 1. Starting parameters for the fluids used in the aqueous alteration models reported in this work. The composition of the reactant rock is shown in Table 2.

| Model code | Temperature (°C) | $Log_{10}$ $fCO_2$ (bar) | $Log_{10}$ $fO_2$ (bar) | pH | ∑C (mol $kg^{-1}$ $H_2O$) |
|---|---|---|---|---|---|
| A | 20 | −0.3 | −4.83 | 4.04 | 0.02 |
| B | 20 | 0 | −4.83 | 3.90 | 0.038 |

Table 2. Composition (in wt%) of the prealtered ALH 84001 rock used as the reactant in the model, modified from Mittlefehldt (1994), using 98.9 vol% orthopyroxene, 1 vol% maskelynite, and 0.1 vol% apatite. Sulfur and chlorine were added from Lodders (1998).

| Oxide (wt%) | ALH 84001 host |
|---|---|
| $SiO_2$ | 53.78 |
| $Al_2O_3$ | 1.01 |
| $Fe_2O_3$ | 0.82 |
| FeO | 16.92 |
| MnO | 0.48 |
| MgO | 24.85 |
| CaO | 1.77 |
| $Na_2O$ | 0.10 |
| $K_2O$ | 0.006 |
| $P_2O_5$ | 0.07 |
| S (ppm) | 110 |
| Cl (ppm) | 8 |
| Total | 99.82 |

$CO_2$ is the most abundant gas in the Martian atmosphere at present (Owen et al. 1977; Mahaffy et al. 2013). Initial $CO_2$ fugacities ($fCO_2$) of 0.5 bar (*Model A*) and 1 bar (*Model B*) were chosen for the system, and the amount of $CO_2$ in the reactant water (Table 1) was allowed to vary throughout the model run after the initial equilibration with the $CO_2$ atmosphere, simulating an environment in relatively poor communication with the atmosphere (Halevy et al. 2011). Specifically, the models were treated as closed systems to $CO_2$, where $CO_2$ was a limiting factor: $CO_2$ used in carbonate formation and other reactions was not replenished. A $pCO_2$ of 1 bar appears to be consistent with the early Martian atmospheric pressure estimated by global circulation models which allow for transient liquid water on the surface (Wordsworth et al. 2013), and near the upper limit to account for ancient crater sizes (Kite et al. 2014), although lower atmospheric pressures (<400 mbar; Cassata et al. 2012) have been proposed for the surface of the early Martian atmosphere. An amount of $O_2$ equal to the pressure existing in the current Martian atmosphere ($pO_2 \approx 1.45 \times 10^{-5}$ bar; Mahaffy et al. 2013) was also included in the initial composition. Other atmospheric species (such as $N_2$ and $SO_2$) were not introduced into the initial composition of the reactant fluid in the models, as the early Martian atmosphere was most likely principally composed of $CO_2$ (Pollack et al. 1987; Jakosky and Phillips 2001; Wordsworth et al. 2013), although relatively large partial pressures of other constituents (e.g., $SO_2$; Halevy et al. 2007) have been proposed to have coexisted with $CO_2$.

## Physical Model

As opposed to the alteration models assuming whole rock chemical equilibrium in the ALH 84001 system or fixed water to rock ratios (W/R) (e.g., Niles et al. 2009; Van Berk et al. 2011), here we used a one-dimensional (1-D) flow model to mimic dissolution–precipitation reactions occurring with groundwater percolation. We assumed that the source of cations for the minerals precipitated was the dissolved orthopyroxenite host rock. An external source for cations, such as the dissolution of an overlying carbonate-rich deposit, could potentially produce the mineralogy observed in ALH 84001, but would ultimately not address the primary source of cations. In the model, a small parcel ($10^{-6}$ kg) of unreacted rock was titrated into a fixed amount (~1 kg) of initial fluid initially in equilibrium with the atmosphere, and the rock–fluid–gas system reached equilibrium.

Subsequently, all mineral precipitates in the equilibrium assemblage were removed from the system, and another small parcel of rock was titrated. As such, at each titration step, the system achieved local equilibrium, but was out of equilibrium with the host rock and minerals precipitated in preceding steps. In this simple 1-D reactive-transport model, W/R is the mass ratio of the initial amount of fluid to the total sum of reacted rock with each titration step. W/R decreased with successive titration steps as the total amount of reacted rock increased, effectively simulating the fluid infiltration pathways in natural systems. Minerals precipitated at high W/R were formed at low degrees of alteration, and minerals precipitated at low W/R were formed with pervasive and extensive alteration of the host rock.

An added advantage of 1-D flow models is that $fCO_2$ below those specified by the initial conditions were also tested for their potential to precipitate phases of interest in the system, as all mineral precipitates (including $CO_2$-sequestering carbonates) were removed from the system as the fluid percolated unaltered host rock, thereby decreasing the $fCO_2$ of the fluid.

To investigate the effect of evaporation (an origin for the zoned carbonates expounded by McSween and Harvey [1998] and Warren [1998]) on forming secondary minerals, and the composition of the precipitated carbonates, water was isothermally removed in incremental steps from the system at $\log_{10}$ W/R = 3, 2, 1, and 0, until activity coefficients could not be determined by extended Debye–Hückel theory (at high ionic strengths, typically at 90–99% $H_2O$ evaporated). $CO_2$ and other gas compounds were still allowed to exchange with the fluid and be incorporated into mineral precipitates. We assumed that equilibration between the minerals precipitated and evaporating fluid was kinetically slower than the formation of mineral precipitates from the evaporating fluid. As in the percolation experiments, minerals formed were removed from the system to prevent back-reaction between the solid fraction and the remaining fluid.

## RESULTS

### 1-D Infiltration Models

The resulting carbonate compositions precipitated in the flow models are summarized in carbonate ternary diagrams (Figs. 1b and 1c). In both 1-D flow models, the carbonate compositions progressed from pure $FeCO_3$ to pure $CaCO_3$ along the $FeCO_3$-$CaCO_3$ join. However, the system initially equilibrated with 1 bar $fCO_2$ (Model B) resulted in a compositional migration to higher Mg content (~$Fe_{67.9}Mg_{20.5}Ca_{9.6}Mn_{2.0}(CO_3)$; Fig. 1c), coinciding with a peak of carbonate production rate in the host rock (~30 wt% of alteration phases at $\log_{10}$ W/R = 2.05; Fig. 2b). This composition falls in range of some carbonate compositions observed in ALH 84001 (Fig. 1a), whereas the system initially equilibrated with 0.5 bar $fCO_2$ (Model A) did not produce Mg-bearing carbonates (Fig. 1b) like the majority of those in the meteorite. A summary of the carbonate compositions produced at specific W/R for each of the models is given in Table 3. Figure 2 shows a comparison of the rates of carbonate and other secondary minerals precipitated in models in relation to the W/R; maximum amounts of carbonate produced were similar across the models, but the larger amount of $CO_2$ in *Model B* extended the range of carbonate precipitation to lower W/R (compare Figs. 2a and 2b), allowing for the precipitation of more magnesian carbonates as Mg from the host rock was dissolved. $Mg^{2+}$, $Ca^{2+}$, $Fe^{2+}$, and $Mn^{2+}$ were precipitated from the fluid as carbonates (Fig. 2) while $CO_2$ and carbon-bearing species were available in solution ($\sum$C in Fig. 3), signifying that the limiting factor to carbonation in this system was the supply of dissolved $CO_2$ (more than ~$2 \times 10^{-4}$ mol $kg^{-1}$ $H_2O$ of total carbon-bearing species, $\sum$C in Fig. 3, was needed to maintain the carbonation precipitation).

During the peak of carbonate production and while carbonates remained abundant minerals in the system ($\log_{10}$ W/R $\approx$ 4.1–2.2 in *Model A*, and $\log_{10}$ W/R $\approx$ 4.1–1.8 in *Model B*), pH remained buffered and relatively unchanged, near neutral values (Fig. 3).

Carbonate mineralization decreased sharply at $\log_{10}$ W/R $\approx$ 2.2 and 1.8 in *Models A* and *B*, respectively (Fig. 2), also marking a change in redox, $fO_2$, and pH conditions, as the initially oxidized fluid became strongly basic (pH > 10, Fig. 3) and more reduced (from Eh = 0.36 V [*Model A*] and Eh = 0.38 [*Model B*] at the height of carbonate precipitation, to −0.30 V [*Model A*] and Eh = −0.42 [*Model B*] at the peak of magnetite precipitation), coinciding with the increased precipitation of talc, chlorite, and alabandite (MnS), which do not occur in the meteorite (Fig. 2). This is revealed by the elevated concentrations of $H_2$ (Fig. 4) and decreased $fO_2$ of the fluid (Fig. 5). $H_2$ was produced from the reduction of $H_2O$, and the oxidation of the Fe endmember of the orthopyroxene (orthopyroxene in ALH 84001 is ~$En_{70}Fe_{27}$) with water while precipitating magnetite:

$$3FeSiO_3(\text{ferrosilite}) + H_2O\ (l) \rightarrow Fe_3O_4\ (\text{magnetite}) + H_2\ (g) + 3SiO_2\ (aq) \quad (1)$$

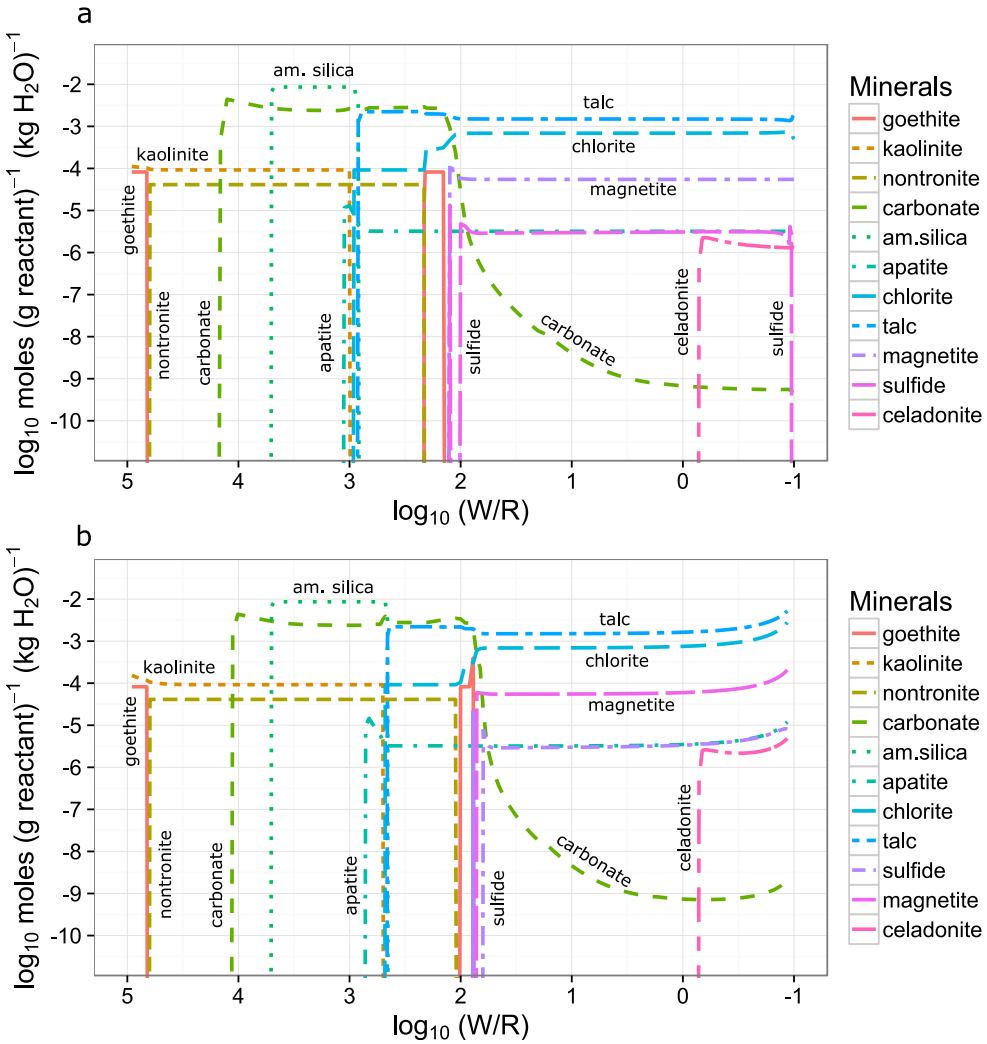


Fig. 2. Secondary mineral precipitates as a function of increased water–rock interaction (i.e., decreasing W/R) in the 1-D flow models. Notice that the ordinate units are $\log_{10}$ moles per gram of titrated rock per kilogram of initial liquid. a) *Model A* (low $CO_2$); b) *Model B* (high $CO_2$).

Although magnetite was stable at lower W/R and higher pH, at higher W/R, above the redox and pH shift, goethite (α-FeO(OH) was the stable Fe-oxi (hydroxi)de (Figs. 2 and 5). The change in redox was controlled by the depletion of dissolved $CO_2$: at high W/R, siderite and ankerite were major sinks of Fe(II) (Figs. 1–3), but at lower W/R, Fe in solution was precipitated as Fe(III) in goethite and magnetite (Figs. 2 and 3).

The progressive alteration of the host rock with continued percolation of the reactant fluid (read from high to low W/R in Fig. 2) shows that prior to the peak in carbonate production, amorphous silica ($SiO_2$) was the alteration mineral preferentially precipitated, and $\sum Si_{(aq)}$ (total Si-bearing species in solution) increased until carbonation stopped (Fig. 3). At this point, $\sum Si_{(aq)}$ was removed as phyllosilicates and other hydrated silicate minerals (Fig. 2), which also acted as sinks for dissolved species of $Mg^{2+}$, $Ca^{2+}$, $Fe^{2+}$, $Mn^{2+}$, $Al^{3+}$ (Fig. 3), $K^+$, and $Na^+$. (Formulae of these minerals, as used in the CHIM-XPT thermodynamic database are reported in the supporting information Table S2.) Most of the chlorite precipitated was the "Al-free chlorite" endmember with a formula of $Mg_6Si_4O_{10}(OH)_8$, compositionally similar to serpentine and talc).

$K^+$ and $Na^+$, although minor elements in ALH 84001 primarily forming the maskelynite, were particularly concentrated in the alteration fluid at low W/R. Chloride salts, which would be major sinks for $K^+$ and $Na^+$, did not form despite the relatively high concentration of Cl in the fluid at low W/R (Fig. 3),

Table 3. Compositions of the carbonates and carbonate wt% of secondary minerals produced in the alteration models. Carbonate wt% for the evaporation models is the total precipitated carbonate from the beginning of evaporation at the specified W/R, until the maximum amount of water able to be evaporated from the system was removed (see text). For 1-D models, carbonate wt% is the carbonate precipitated at the specified W/R.

| $Log_{10}$ W/R | Carbonates (wt%) | $H_2O$ evaporated (wt% $H_2O$) | $Log_{10}$ $fCO_2$ (bar) | pH | Carbonate composition (mol%) | | | |
|---|---|---|---|---|---|---|---|---|
| | | | | | $FeCO_3$ | $CaCO_3$ | $MgCO_3$ | $MnCO_3$ |
| Model A (0.5 bar initial $fCO_2$) 1-D flow | | | | | | | | |
| 3 | 35.1 | N.A. | −0.9 | 6.7 | 90.0 | 0 | 0 | 10.0 |
| 2 | 0.3 | N.A. | −8.9 | 10.9 | 0 | 26.1 | 0 | 73.9 |
| 1 | $4 \times 10^{-5}$ | N.A. | −13.2 | 12.5 | 0 | 100.0 | 0 | 0 |
| 0 | $7 \times 10^{-6}$ | N.A. | −15.6 | 13.4 | 0 | 100.0 | 0 | 0 |
| Model A isothermal evaporation | | | | | | | | |
| 3 | 23.3 | 89.5 | 0 | 6.6 | 0.1 | 24.0 | 72.1 | 3.8 |
| 2 | 85.9 | 99.6 | −16.8 | 13.0 | 0 | 100.0 | 0 | 0 |
| 1 | 73.5 | 99.8 | −19.8 | 13.9 | 0 | 100.0 | 0 | 0 |
| 0 | 100 | 96.9 | −19.6 | 14.0 | 0 | 100.0 | 0 | 0 |
| Model B (1 bar initial $fCO_2$) 1-D flow | | | | | | | | |
| 3 | 33.1 | N.A. | −0.2 | 6.1 | 100 | 0 | 0 | 0 |
| 2 | 29.1 | N.A. | −2.3 | 7.9 | 69.7 | 9.9 | 18.4 | 2.0 |
| 1 | $4 \times 10^{-5}$ | N.A. | −13.2 | 12.5 | 0 | 100 | 0 | 0 |
| 0 | $7 \times 10^{-6}$ | N.A. | 15.6 | 13.4 | 0 | 100 | 0 | 0 |
| Model B isothermal evaporation | | | | | | | | |
| 3 | 17.0 | 89.5 | 0 | 6.6 | 0.1 | 24.0 | 72.1 | 3.8 |
| 2 | 72.6 | 97.5 | −0.1 | 7.2 | 1.7 | 0.3 | 0.8 | 97.3 |
| 1 | 77.2 | 99.5 | −18.6 | 14.0 | 0 | 100.0 | 0 | 0 |
| 0 | 100 | 96.6 | −19.6 | 14.0 | 0 | 100.0 | 0 | 0 |

N.A. = not applicable.

although Fe-celadonite ($KFeAlSi_4O_{10}(OH)_2$) sequestered $K^+$ at very low W/R (Fig. 2).

### Isothermal Evaporation

Isothermal evaporation of the water brought significant changes to the carbonate compositions (Fig. 1) and mineral assemblages precipitated (Figs. 6 and 7). Generally, the proportion and mass of carbonate precipitated increased in both *Models A* and *B* at all W/R (Figs. 6 and 7). Evaporation at high W/R produced diverse Ca-Mg-Fe-Mn carbonates (Figs. 1b, 1c, 6a, 7a–b) but only Ca carbonates were produced by evaporating water at low W/R (Figs. 6b–d and 7c–d), i.e., with pervasive alteration of the host rock.

## DISCUSSION

### Carbonate Compositions

Out of all the models tested, the most successful in producing sufficient carbonate proportions and diverse compositions approximating the carbonates in ALH 84001 was *Model B* followed by evaporation from $log_{10}$ W/R = 3 (Figs. 1c and 7a). This resulted in carbonates falling in a range of carbonate compositions, including siderite, calcite, and intermediate compositions between the three major endmembers at a range of W/R (Fig. 6). No intermediate carbonates containing Ca, Fe, and Mg precipitated in the 1-D flow or evaporation models for *Model A* (Fig. 1b). Arguably, the higher carbonate in solution in *Model B* (Fig. 3b) allowed the carbonation reaction to occur (Fig. 2b), while Si was elevated in the solution (Fig. 3b); cations were effectively removed from the solution as hydrated silicates (especially chlorite and talc) in *Model A* (Fig. 2a). For purposes of the discussion, we concentrate on *Model B*.

While the sequence of precipitated carbonates in the models (starting with $FeCO_3$ at high water–rock ratio, progressing to Fe-Ca-Mg carbonates at mid high W/R, and finally calcite at low W/R [Fig. 1c]) is in a different order from the zonation pattern observed in ALH 84001 (Ca-rich cores with increasing Fe content toward the exterior, followed by sideritic and magnesite rims), we hypothesize that the first fluids that arrived at the nucleation sites for the carbonates were relatively low W/R fluids ($log_{10}$ W/R $\leq$ 1.8; Fig. 1c) that had percolated through the fractures and pores of the dry host rock and the dry (but actively being weathered) stratigraphically

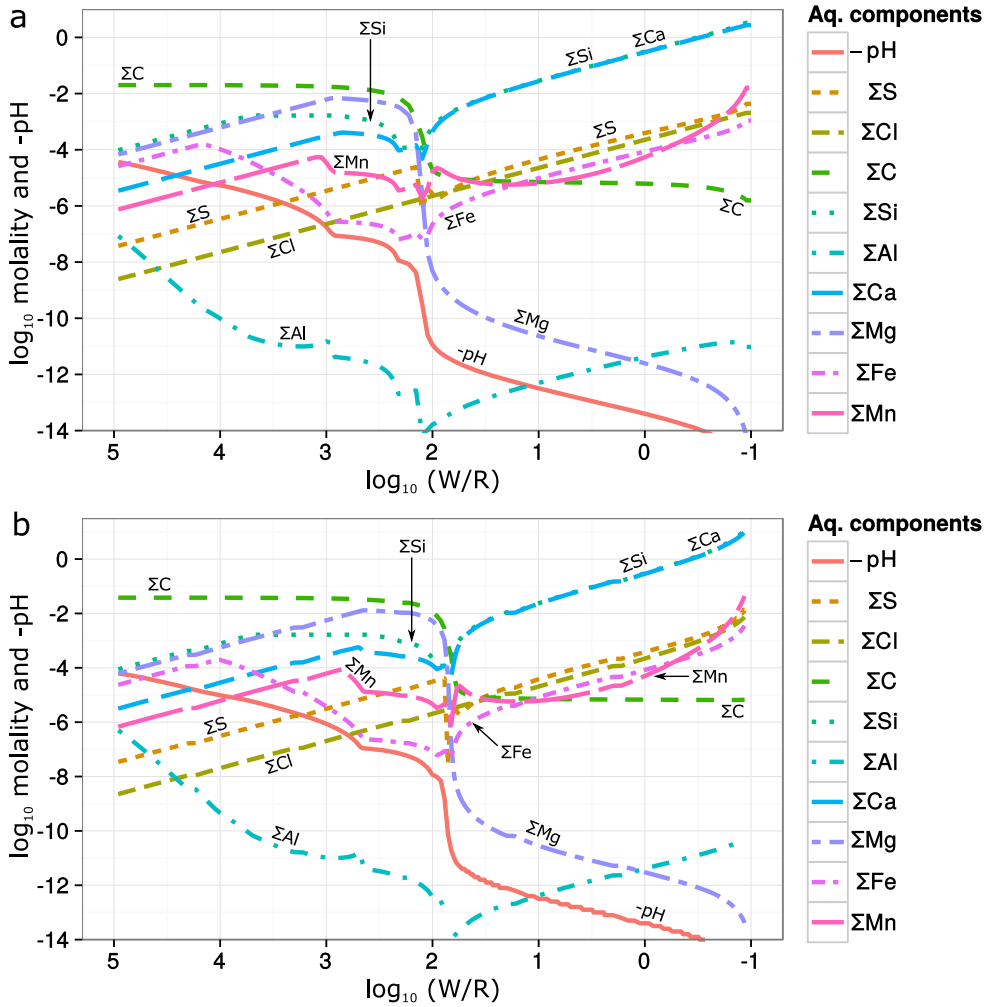


Fig. 3. Concentrations of dissolved aqueous components and pH in the fluids of the 1-D flow models. a) *Model A* (low $CO_2$), b) *Model B* (high $CO_2$). "Components" refers to all aqueous species containing the particular element, e.g., ∑S includes $SO_4^{2-}$, $HS^-$, etc.

overlying rock of similar composition, and precipitated the first Ca-rich crystals of the cores. Subsequent fluids percolated the fractures experiencing less reaction with the overlying host rock as porosity was clogged by hydrated silicates produced by the first low W/R fluids. Alternatively, the groundwater table rose to the level of the ALH 84001 host as a response to recharge from the percolating fluids. As a result, increasingly Fe- and Mg-carbonates would precipitate at $\log_{10}$ W//R ≈ 1.8–2.2, culminating in pure $FeCO_3$ (at $\log_{10}$ W/R > 2.7; Fig. 1c). Finally, evaporation of the relatively abundant and dilute fluids that had experienced little interaction with the host rock would produce the more voluminous Mg carbonates (Figs. 1c, 7a–b). The Mg-rich precursor carbonate huntite is required prior to transformation to the observed magnesite, but this may also explain the Sr enrichment observed in the meteorite by Beard et al. (2013). Though the weathering of Mg silicates may increase Sr/Ca ratios of the permeating alteration fluid, Sr also substitutes readily for Ca in the relatively open-latticed structure of huntite, in comparison to magnesite (Dollase and Reeder 1986; Stanger and Neal 1994). Unfortunately, recognizing whether the Mg carbonate in ALH 84001 is recrystallized, postdepositionally transformed huntite is not trivial. Huntite occurs as an evaporitic near-surface weathering product and as a fine-grained diagenetic mineral in dissolution pores of ultramafic rocks (e.g., Kinsman 1967; Stanger and Neal 1994; Akbulut and Kadir 2003), but is metastable (Garrels et al. 1960; Kinsman 1967), and is replaced in time by magnesite–dolomite or dolomite–calcite, with no diagnostic habits or pseudomorphs preserved

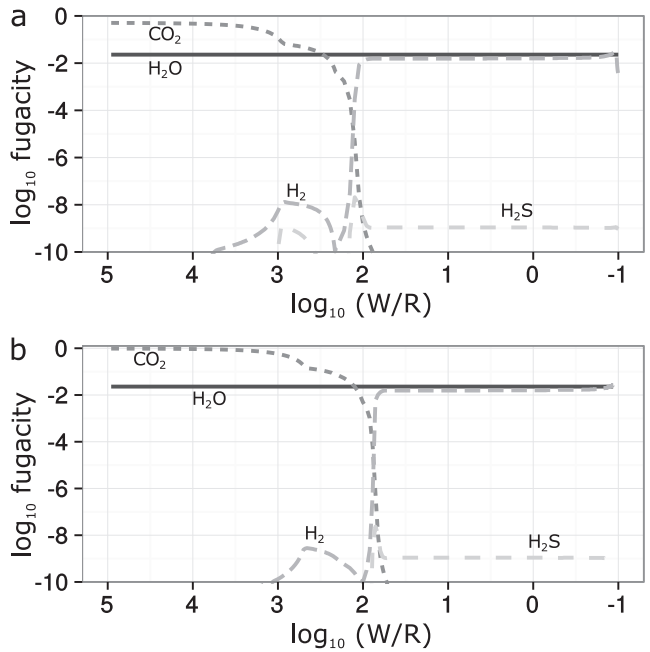


Fig. 4. $Log_{10}$ fugacity of the dissolved gases in the alteration fluids as a function of increased water–rock interaction (i.e., decreasing W/R) in a) *Model A* (low $CO_2$); b) *Model B* (high $CO_2$).

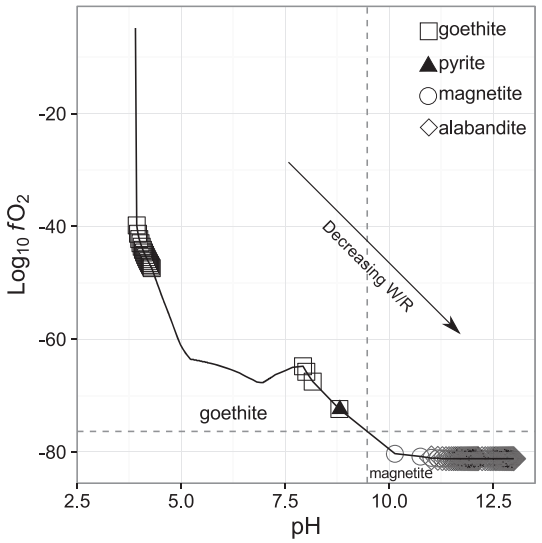


Fig. 5. Oxides and sulfides precipitated in 1-D flow *Model B* (high $CO_2$), as a function of changing pH and $fO_2$ of the permeating fluid (solid line) with increased rock reacted (decreasing W/R). Dashed lines divide the observed stability fields for goethite and magnetite in the system. Goethite only precipitated in the top left quadrant, and magnetite only in the bottom right quadrant.

(Kinsman 1967). Possibly, the shock event(s) that occurred after carbonate deposition and that mobilized maskelynite in the meteorite could also have transformed huntite to magnesite.

## Hydrated Silicates and Other Alteration Phases

Alteration phases other than carbonates were abundant even at the peak of carbonate precipitation in both 1-D flow models (Fig. 2; Table 3). In contrast, in the meteorite, carbonates form almost the entirety of the alteration assemblage observed, meaning that if the carbonates in ALH 84001 formed under the conditions tested, this would only have been possible if a mechanism had been in place to dissolve and remove (or inhibit the formation of) secondary phases other than carbonate. Conceivably, shock could have transformed any existing smectites back to olivine and pyroxene, although direct evidence for this transformation does not exist in the meteorite. We note, however, that silica glasses are observed in the meteorite (e.g., Scott et al. 1997); the silica phases were possibly contemporaneously precipitated with the carbonates, and shock-mobilized thereafter (Greenwood and McSween 2001). Low-temperature equilibrium conditions inhibit the precipitation of Mg carbonate (e.g., Hänchen et al. 2008; Saldi et al. 2009), so we consider it unlikely that pervasive equilibrium dissolution of the host rock by the alteration fluid and subsequent precipitation of the carbonates occurred. The lack of textural and mineralogical evidence for intensive fluid interaction in ALH 84001 has been noted (Treiman and Romanek 1998), and the compositional and isotopic zonation of the carbonates in the meteorite is strongly indicative of disequilibrium conditions (e.g., Harvey and McSween 1996; Treiman 1997; Valley et al. 1997).

While kaolinite, nontronite, and celadonite are not unusual phyllosilicates in low-temperature aqueous alteration systems on Earth, the precipitation of talc and chlorite in the models under these conditions (Fig. 2) is unusual and requires further justification. Talc forms, and is stable, at ambient conditions in laboratory tests (Bricker et al. 1973; Tosca et al. 2011), and authigenic sedimentary talc is reported in (among other carbonate-rich deposits) Neoproterozoic carbonate layers in Svalbard and the Yukon (Tosca et al. 2011; and references therein). Apparently, pH exerts a strong control on the formation of talc, preferentially precipitating in alkaline conditions (Tosca et al. 2011), in line with the talc computed in the batch equilibrium models. (Alternatively, thermochemical data available to us for nontronite and other smectites are as yet deficient, especially considering that they are complex solid solutions.) From the observations of soil formation in ancient (~4.2 Ga; Farley et al. 2014) rocks in Gale crater on Mars, mostly from the low-temperature chemical weathering of olivine (Retallack 2014), talc minerals may have precipitated from

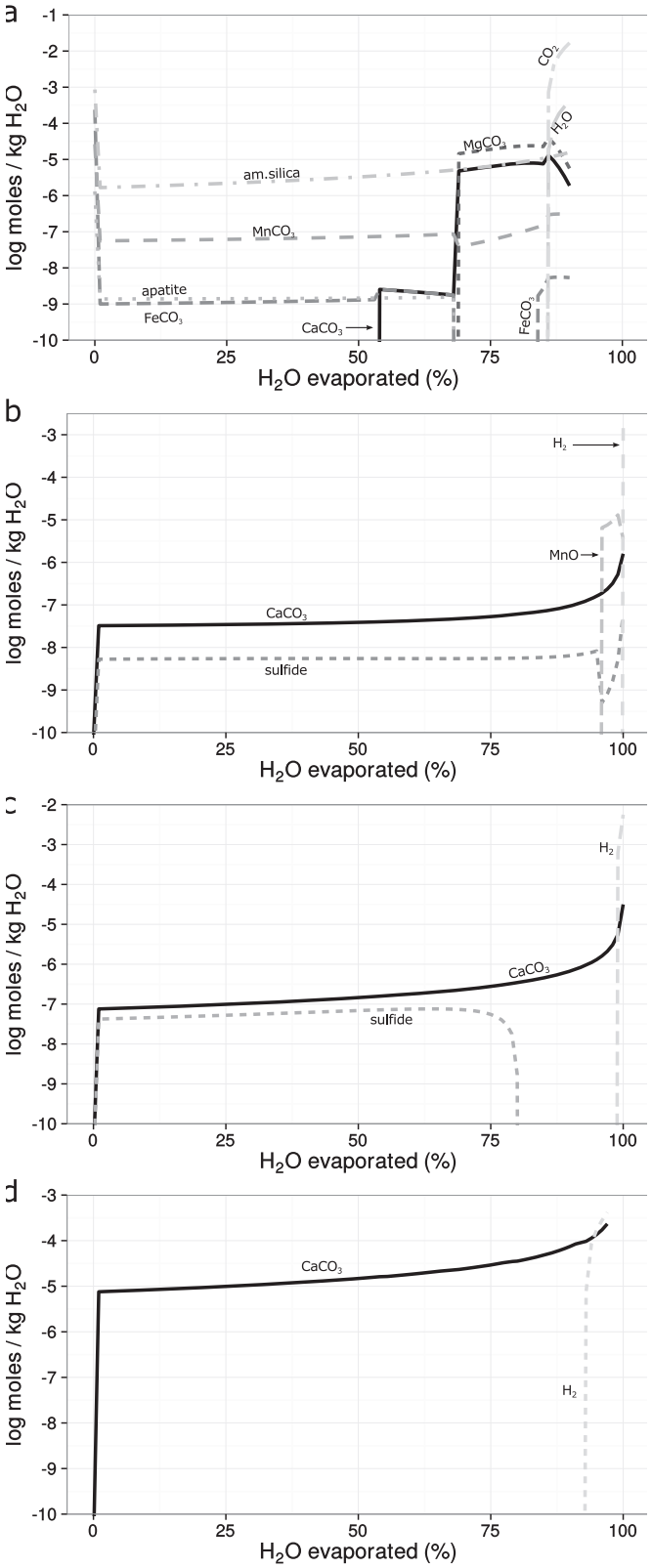


Fig. 6. Phases produced as a function of the amount of water evaporated (removed) from the system in *Model A* (low $CO_2$): a) evaporation starting at $\log_{10}$ W/R = 3; b) starting at $\log_{10}$ W/R = 2; c) starting at $\log_{10}$ W/R = 1; d) starting at $\log_{10}$ W/R = 0. Back-reaction and re-equilibration between the remaining water and the rock were prohibited (see text).

weathered pyroxene under low-temperature, basic conditions. Low-temperature chlorite is also relatively uncommon on Earth as it tends to form in diagenetic and low-temperature metamorphic environments (and appears associated with craters on Mars; Ehlmann and Edwards 2014), but is, e.g., thought to be authigenic in weathered sedimentary deltaic sandstones at 20–40 °C in South Texas (Grigsby 2001).

Goethite (FeO(OH)) was the first phase to precipitate from the fluid in both models ($\log_{10}$ W/R > 4.8; Fig. 2). Goethite and carbonate coprecipitated and were stable in a small window ($\log_{10}$ W/R ≈ 2–1.9; Fig. 2), as were carbonate with magnetite and sulfides ($\log_{10}$ W/R < 1.9; Fig. 2). Hematite grains are ubiquitous in the carbonates of ALH 84001, but goethite has not been detected in the meteorite (Steele et al. 2007). However, goethite and hematite are close in stability, and either form from the common metastable ferrihydrite ($\sim 5Fe_2O_3 \cdot 9H_2O$) precursor at room temperature, the determining factor being pH (Schwertmann and Murad 1983). At pH of 2–5 and 10–14, goethite tends to precipitate, while hematite is favored at pH 5.5–9.5 (Schwertmann and Murad 1983; Cudennec and Lecerf 2006). On the other hand, goethite that coprecipitated with the carbonates (Fig. 2) at moderately alkaline pH (Fig. 5) may have been transformed to the hematite observed in the meteorite by an event postdating aqueous alteration and evaporation involving higher temperatures, i.e., the postimpact transformation of siderite into magnetite, as suggested by Brearley (2003). Cudennec and Lecerf (2005) reported that the topotactic (solid-state crystallographic) thermal dehydroxylation of pure goethite to hematite occurs at 260–320 °C, with no intermediate phase being produced. Shock metamorphism as that which almost certainly occurred after the deposition of the carbonates (and as evidenced by the fragmentation of the carbonates and emplacement of feldspathic melt glass within them [Treiman 1995, 1998]) would also have the effect of transforming carbonates to macromolecular carbon and graphite (Steele et al. 2007, 2012a, 2012b). Goethite and magnetite did not coprecipitate in the models (Fig. 2). In this regard, the magnetite crystals occurring in ALH 84001 would not have necessitated transportation into the host rock by allocthonous fluids, as e.g., Thomas-Keprta et al. (2009) have previously suggested. We note that much work has been carried out to determine the origin of the magnetite crystals in ALH 84001 (Scott 1999; Thomas-Keprta et al. 2000, 2009; Barber and Scott 2002; Brearley 2003; Golden et al. 2004; Treiman

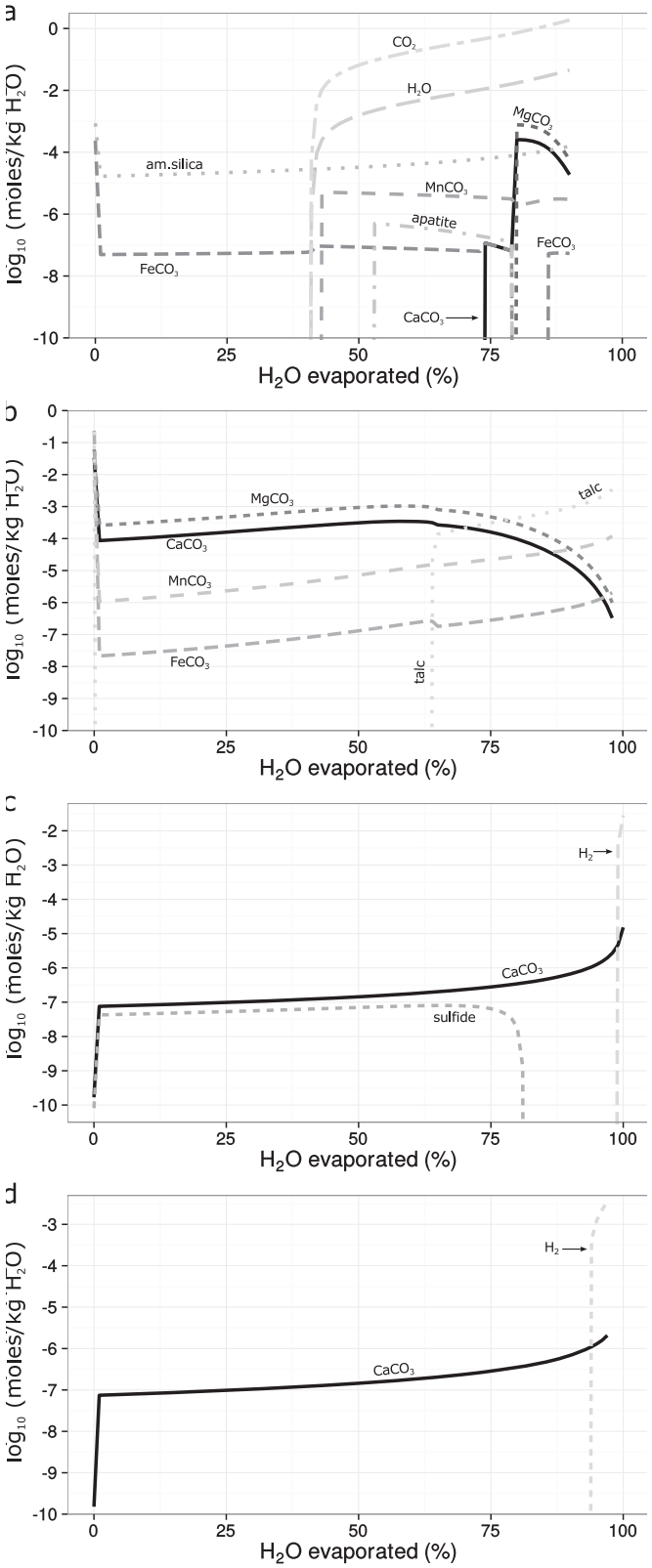


Fig. 7. Phases produced as a function of the amount of water evaporated (removed) from the system in *Model B* (high $CO_2$): a) evaporation starting at $\log_{10}$ W/R = 3; b) starting at $\log_{10}$ W/R = 2; c) starting at $\log_{10}$ W/R = 1; d) starting at $\log_{10}$ W/R = 0. Back-reaction and re-equilibration between the remaining water and the rock were prohibited (see text).

and Essene 2011). Here, an abiogenic, low-temperature pathway from the oxidation of Fe-pyroxene, involving the production of $H_2$ (Fig. 4), was able to precipitate magnetite (Fig. 2) without direct participation of carbonate minerals in the reaction (Reaction 1). A serious limit on this hypothesis is the lack of observed hydrated silicates in ALH 84001, and calculated to have been stable in the 1-D flow models while magnetite was being precipitated (Fig. 2). Incidentally, magnetite formed in the reduction reaction could catalyze the reduction of $CO_2$ to form hydrocarbons (Zolotov and Shock 1999), e.g., the variable methane the *Curiosity* rover has recently measured in the atmosphere at Gale Crater (Webster et al. 2015). The possible abiotic production of $CH_4$ on early Mars has been discussed extensively, particularly in its role and abundance in the atmosphere (e.g., Chassefière and Leblanc 2011a, 2011b). Similarly, $H_2$ and $CO_2$ have been advocated as potential greenhouse agents in the early Martian atmosphere which enabled water to stay above the freezing point (e.g., Hirschmann and Withers 2008; Ramirez et al. 2014). However, as mentioned above, $CH_4$-$H_2O$-$CO_2$ equilibration is inhibited at low temperatures (and disallowed in our model), and so a kinetic barrier prohibits the formation of $CH_4$ from the reduction of $CO_2$ and $H_2O$ (e.g., Seewald et al. 2006; McCollom 2013).

## Isotope Considerations

Rubidium and strontium systematics in ALH 84001 were used to suggest pre-existing phyllosilicates as the origin of $^{87}Rb/^{86}Sr$ enrichment (Beard et al. 2013). On the basis of the reaction models carried out here it appears that phyllosilicates kaolinite and smectite plus silica could have formed above the host rock of ALH 84001 (Fig. 2) if fluids permeating downward from the surface produced the carbonates, but the silicates would not have necessarily predated the carbonates significantly.

Although our models do not account for the stable isotope observations in ALH 84001, we note that the C and O isotopic variability in the carbonate rosettes (e.g., Romanek et al. 1994; Valley et al. 1997; Leshin et al. 1998; Eiler et al. 2002b; Niles et al. 2005) and H isotope observations (Leshin et al. 1996; Eiler et al. 2002a) are plausibly consistent with the results of the "1-D flow and evaporation" model we present. Specifically, the model did not allow for chemical equilibrium with the bulk host rock and the precipitated minerals, so it permits the variation of stable isotopes along the

alteration path and among the mineral compositions precipitated, as well as isotopic disequilibrium between the host rock and the secondary precipitates. While the $\delta^{18}O$ in the rosettes increases from core to rim (from Ca- to Mg-rich carbonate; Valley et al. 1997; Leshin et al. 1998; Eiler et al. 2002b), a kinetic isotope fractionation pattern often observed in carbonates formed in evaporative freshwater environments on Earth (e.g., Fornaca-Rinaldi et al. 1968; Hendy 1971), a reversal toward lower $\delta^{18}O$ is observed with increased evaporation in briny waters (Sofer and Gat 1975). However, the alteration fluid modeled here was very low in Cl and $SO_4^{2-}$ (which would reduce the equilibrium fractionation of oxygen). The detailed analysis (Halevy et al. 2011) of the relationship between the carbonate compositions in ALH 84001, and the C and O stable isotope variations affected by evaporation, $CO_2$ degassing, and kinetic isotope effects, is in agreement with an evaporative environment controlling the increase in $\delta^{18}O$ and $\delta^{13}C$ from core to rim.

Studies (Leshin et al. 1996; Sugiura and Hoshino 2000; Eiler et al. 2002a; Boctor et al. 2003) have shown the carbonates in ALH 84001 to be deuterium-enriched ($\delta D_{VSMOW}$ = 331–1196 ‰; Boctor et al. 2003) and the most water-rich phases (0.4–1.1 wt. % $H_2O$; Boctor et al. 2003) in an otherwise very dry rock (0.08 wt% $H_2O$; Leshin et al. 1996). As discussed above, we computed the generation of $H_2$ from the formation of magnetite in the 1-D flow models. To our knowledge, high-resolution spatial analyses of the hydrogen isotopic variability within the rosettes have not been carried out, but if the magnetite formed through the process described above, $\delta^2H$ in the carbonates containing magnetite may increase from core to rim congruently with the $\delta^{18}O$ increase, as is observed in evaporative environments on Earth (e.g., Barnes and Allison 1988). Of particular interest regarding the O and H isotope variations in the carbonates are the fractionations that are observed as a function of depth and evaporation regimes in soils (Barnes and Allison 1988; and references therein). Extreme differences of over ± 40 ‰ in both $\delta^{18}O_{SMOW}$ and $\delta^2H_{SMOW}$ are observed in <5 cm depth under isothermal evaporation conditions. Future work might seek to link the presence of magnetite to carbonate compositions and their covarying isotopic signatures together with percolation depth and evaporation regime profiles.

## Comparison to Other Geochemical Models of the Carbonates in ALH 84001

Other workers have investigated the distinctive carbonates of ALH 84001 with thermochemical models. Kopp and Humayun (2003) argued that dissolution of the carbonate concretions, subsequential to their deposition on Mars, produced the characteristically zoned siderite–magnesite–siderite rims, and that this process plausibly occurred in Antarctica, during the terrestrial residence time of the meteorite. With the use of a kinetic dissolution–precipitation model, they contended that low amounts of meltwater infiltrating the rock dissolved Mg and Fe from the native carbonates, and subsequent sublimation of the fluids at low $fO_2$ ($<10^{-69}$ bar at 25 °C) produced the magnetite crystals and carbonate rims. While a suggestive argument, we emphasize that hematite has also been reported in the carbonate rosettes of ALH 84001 (Steele et al. 2007), indicating that $fO_2$ may have been different from that described in their model. To our knowledge, no other carbonate-bearing Antarctic meteorite, Martian or otherwise, has developed similar magnesite rims around pre-existing carbonate, despite the relative abundance of Antarctic hydrous Mg carbonates on fusion crusts and cracks of chondrites (e.g., Velbel et al. 1991), which do not occur in ALH 84001. (We point out, however, that the Tatahoiune diogenite does contain terrestrial calcite "rosettes," formed over 60 years of exposure to warm semiarid conditions; Barrat et al. 1999.) Niles et al. (2005) also offered evidence against an Antarctic origin for the magnesite, based on their measurements of high $\delta^{13}C$ values (46 – 65 ‰). Finally, Niles et al. (2009) and Van Berk et al. (2011) suggested that decreasing $pCO_2$ caused the carbonates in ALH 84001 to precipitate, presumably as an upwelling $CO_2$-charged fluid degassed and increased in pH. In a broad sense, our 1-D flow model is consistent with theirs, given that the Fe carbonates precipitated at $fCO_2$ = 0.93 – 0.22 bar and the Mg-rich carbonates precipitated at $fCO_2 = 5 \times 10^{-2}$–$5 \times 10^{-3}$ bar (in *Model B*, Figs. 1c, 2b, and 4b), compared to the initial reactant fluid with $fCO_2$ = 1 bar. However, our mechanism to remove $CO_2$ from the system consisted of water–rock reaction with fluids percolating from the surface, rather than an externally controlled parameter, and we have considered the role of compositional changes to the percolating fluid as a result of fluid–rock dissolution–precipitation processes as well as the role of evaporation on the secondary assemblage. Notably, near-neutral pH and relatively low temperatures were required to produce carbonates in both the high and low $fCO_2$ thermochemical models run in this study.

The low-temperature conditions we envision for the precipitation of the carbonate concretions in ALH 84001 are similar to those leading to sphaerosiderite precipitation in terrestrial soils (Ludvigson et al. 2013), and unlike those that formed the zoned Ca-Fe-Mg carbonate globules in basalts, and crustal and mantle

xenoliths in Spitsbergen (Norway; Treiman et al. 2002). Sphaerosiderites are $FeCO_3$ concretions formed mainly by infiltrating meteoric fluids (<30 °C; e.g., Ludvigson et al. 2013), whereas the Spitsbergen carbonate globules were probably precipitated from permeating hydrothermal fluids (50–70 °C) which allowed the direct formation of magnesite (Treiman et al. 2002) instead of requiring a huntite precursor.

**Comparison to Other Ancient Martian Systems**

It is useful to discuss previous work on Martian aqueous systems and observed alteration assemblages to ascertain the validity of our model. Sideritic and Ca-siderite carbonates are observed in the nakhlite group of Martian meteorites (especially Lafayette, Governador Valadares, and Nakhla), and were probably formed from the dissolution of surrounding rocks in a near-surface environment (e.g., Bridges and Grady 2000; Changela and Bridges 2010; Hicks et al. 2014). Clay minerals (saponite) postdate and partially dissolve the carbonates, which are likely metastable (Changela and Bridges 2010; Hicks et al. 2014). A $CO_2$-rich brine that first precipitated the Fe-Ca carbonates in the nakhlites at 150–200 °C, subsequently precipitated the clay minerals as it cooled to ~50 °C (Bridges and Schwenzer 2012), suggesting that the fluid permeating the nakhlites and the associated hydrothermal alteration system were longer lived than the alteration environment of ALH 84001. Similar to the nakhlites, in ALH 84001, clay minerals probably also postdated the carbonates, but furthermore, would have reached saturation in the fluid and thermodynamic stability contemporaneously with the carbonates (Fig. 2).

In a more relevant temperature regime (13 °C), Filiberto and Schwenzer (2013) investigated the potential alteration phases resulting from the alteration of the ancient basalt at Home Plate (Columbia Hills, Gusev Crater), which resulted in assemblages dominated by chlorite or nontronite across all W/R, and only some carbonate (up to ~25 wt% of all secondary products) in fluids with high dissolved initial $\sum C$ (approximately one order of magnitude higher than used in our models). On a first basis, their modeled assemblages appear similar to the ones modeled here, but importantly, the Home Plate basalt composition and the reactant water they used contained significantly more Cl and S, most likely suppressing higher carbonate production in favor of other secondary phases—an unlikely scenario for ALH 84001. Van Berk and Fu (2011), and later, Van Berk et al. (2012), carried out 1-D diffusive mass transport models on olivine-rich host rocks which effectively reproduced the carbonate assemblages at the Comanche outcrop ($Mg_{0.62}Fe_{0.25}Ca_{0.11}Mn_{0.02}CO_3$; Morris et al. 2010) also at Gusev crater, and carbonates and stratigraphically lower phyllosilicates at Nili Fossae (Ehlmann et al. 2008). Our model results, in which infiltrating fluids first precipitated mainly silica, then carbonates, and finally progressed to phyllosilicates, are broadly consistent with theirs, indicating that similar $pCO_2$ and temperature conditions (~1 bar $pCO_2$ and < 25 °C), as well as fluid compositions prevailed at the site where ALH 84001 was altered, and at the Comanche outcrop and Nili Fossae. Their phyllosilicate assemblages differed somewhat from the assemblages calculated here: at Nili Fossae, they computed talc, diaspore, chrysotile, greenalite, prehnite, and minor chlorite precipitation at depth, whereas here, talc, chlorite, and minor amounts of magnetite, apatite, and ferroceladonite precipitated toward lower W/R (Fig. 2). This difference is most likely driven by the different host rock compositions, as ALH 84001 is virtually olivine-free, and the host rocks considered by Van Berk and Fu (2011) are relatively olivine-rich. (Although, it is plausible that more olivine was present in the host rock of ALH 84001 prior to the formation of the carbonates, and that the latter mainly replaced the olivine; Treiman 2005.) Another significant difference between their models and ours concerns the progression of carbonate compositions. While here, the carbonates invariably start at the Fe endmember composition at high W/R and progress along the Fe-Ca carbonate join with further percolation (via an excursion to higher Mg content; Figs. 1a and 1b), their carbonate compositions progress from Fe- to Mg-carbonate near the Fe-Mg join and then toward the Ca endmember along the Mg-Ca join, signifying that ankerite compositions, as present in the cores of the rosettes in ALH 84001, would be absent. Recent equilibrium thermochemical models of the Comanche outcrop carbonates (Ruff et al. 2014) also suggested that the carbonate formed from the leaching of the nearby olivine-rich Algonquin outcrop. Finally, mineralogical analyses and geochemical modeling carried out for Yellowknife Bay in Gale crater revealed that mudstones there contained sulfates (basanite and anhydrite) magnetite, hematite, and smectites (possibly saponite) among other components (Vaniman et al. 2014; Bridges et al. 2015). While hematite and magnetite occur in ALH 84001, and dioctahedral smectite (nontronite) was calculated to precipitate while carbonates were stable (Fig. 2), the presence of extensive sulfates at Yellowknife Bay argues against a direct association with substantial carbonate formation. In fact, carbonates are not present above MSL's CheMin's detection limit (>1 wt%) at Yellowknife Bay (Ming et al. 2014; Vaniman et al.

2014). This is supported by the geochemical models of Schwenzer et al. (2016), who use the low carbonate abundances in the Yellowknife Bay sediments as one of their arguments for alteration by a subsurface fluid with low $CO_2$ concentration, rather than an atmospherically derived fluid as was the case for ALH 84001.

## CONCLUSION

Over 30 years since its recovery from Antarctica, ALH 84001 continues to reveal a wealth of information about hydrological and geochemical conditions and surroundings on early Mars. Here we have presented evidence for the conditions under which the carbonate rosettes precipitated, the composition of the fluids that altered the host rock, and the alteration mineralogy of the rocks in the vicinity of ALH 84001, when it was emplaced near the surface of Mars. At low temperature (20 °C) and $pCO_2 \leq 1$ bar, and under local equilibrium conditions with a 1-D fluid flow model, we precipitated a range of carbonate compositions closely resembling those observed in the meteorite, following evaporation. The Ca-Fe carbonates were most likely produced with fluids that reacted with the orthopyroxenite overlying the host of the meteorite (low W/R), and the higher Fe and Mg carbonates reflect subsequent permeation by fluids that experienced little reaction with the orthopyroxenite (high W/R). High Mg carbonate was precipitated by evaporation of the water in the system. Carbonate–evaporite formation was likely a faster process than the equilibration of the alteration fluid with the host rock and the secondary precipitates. The formation of pure magnesite was probably a process that occurred postdepositionally as a result of diagenesis or shock metamorphism from the precursor Mg-rich carbonate, and is beyond the scope of this work. Formation of carbonates in ALH 84001 resulted from relatively limited water–rock interaction to result in maximal production of carbonates relative to Mg-bearing hydrated silicates, and evaporation played a major role in producing the metastable Mg carbonates, possibly crystallizing on the order of days (Bridges et al. 2001). Thus, a short-lived, open, aqueous system appears to be in agreement with the formation of carbonates in ALH 84001.

The production of carbonates in ALH 84001 entails the formation of other secondary phases, which may not be represented in the meteorite or were destroyed or transformed by subsequent shock. As percolating fluids permeated ALH 84001 and the rocks surrounding ALH 84001, fluid compositions evolved, and $pCO_2$ and W/R decreased. Principal minerals produced from high W/R to low W/R were $SiO_2$, goethite, carbonates (siderite, ankerite, huntite, and calcite), kaolinite, nontronite, chlorite, talc, magnetite, and sulfide. Goethite coprecipitated with carbonate, showing that previously observed hematite in the ALH 84001 rosettes (Steele et al. 2007) may come from the transformation of goethite. Similarly, with increased water–rock interaction (lower W/R), magnetite and carbonate were stable, indicating that the carbonates and magnetite in ALH 84001 may have been produced from the same fluid, and generated $H_2$.

*Acknowledgments*—We thank J. Palandri for help with thermochemical modeling and G. J. Retallack for information on talc and zeolite stability in arid soils. The ggtern package by N. Hamilton for R was used for this work. The work presented here benefitted from the comments of A. H. Treiman and three anonymous reviewers. Comments from M. Humayun and E. S. Kite further improved the manuscript. MMD acknowledges funding from the Science and Technology Facilities Council (PhD studentship), Royal Astronomical Society, Lunar and Planetary Institute (Career Development Award) and the Geochemistry Group (Geological Society and Mineralogical Society of Great Britain and Ireland), and SPS acknowledges funding from an Open University Research Investment Fellowship.

*Editorial Handling*—Dr. Justin Filiberto

## REFERENCES

Akbulut A. and Kadir S. 2003. Huntite deposits in the neogene lacustrine sediments of the Cameli basin, Denizli, SW Turkey. *Carbonates and Evaporites* 18:1–9. doi:10.1007/BF03178382.

Arvidson R. S. and Mackenzie F. T. 1999. The dolomite problem; control of precipitation kinetics by temperature and saturation state. *American Journal of Science* 299:257–288. doi:10.2475/ajs.299.4.257.

Arvidson R. E., Squyres S. W., Bell J. F., Catalano J. G., Clark B. C., Crumpler L. S., de Souza P. A., Fairén A. G., Farrand W. H., Fox V. K., Gellert R., Ghosh A., Golombek M. P., Grotzinger J. P., Guinness E. A., Herkenhoff K. E., Jolliff B. L., Knoll A. H., Li R., McLennan S. M., Ming D. W., Mittlefehldt D. W., Moore J. M., Morris R. V., Murchie S. L., Parker T. J., Paulsen G., Rice J. W., Ruff S. W., Smith M. D., and Wolff M. J. 2014. Ancient aqueous environments at Endeavour Crater, Mars. *Science* 343(6169):1248097. doi:10.1126/science.1248097.

Barber D. J. and Scott E. R. D. 2002. Origin of supposedly biogenic magnetite in the Martian meteorite Allan Hills 84001. *Proceedings of the National Academy of Sciences* 99:6556–6561.

Barnes C. J. and Allison G. B. 1988. Tracing of water movement in the unsaturated zone using stable isotopes of

hydrogen and oxygen. *Journal of Hydrology* 100:143–176. doi:10.1016/0022-1694(88)90184-9.

Barrat J. A., Gillet P., Lesourd M., Blichert-Toft J., and Poupeau G. R. 1999. The Tatahouine diogenite: Mineralogical and chemical effects of sixty-three years of terrestrial residence. *Meteoritics & Planetary Science* 34:91–97. doi:10.1111/j.1945-5100.1999.tb01734.x.

Beard B. L., Ludois J. M., Lapen T. J., and Johnson C. M. 2013. Pre-4.0 billion year weathering on Mars constrained by Rb–Sr geochronology on meteorite ALH 84001. *Earth and Planetary Science Letters* 361:173–182. doi:10.1016/j.epsl.2012.10.021.

Bibring J.-P., Langevin Y., Mustard J. F., Poulet F., Arvidson R., Gendrin A., Gondet B., Mangold N., Pinet P., Forget F., Berthé M., Bibring J.-P., Gendrin A., Gomez C., Gondet B., Jouglet D., Poulet F., Soufflot A., Vincendon M., Combes M., Drossart P., Encrenaz T., Fouchet T., Merchiorri R., Belluci G., Altieri F., Formisano V., Capaccioni F., Cerroni P., Coradini A., Fonti S., Korablev O., Kottsov V., Ignatiev N., Moroz V., Titov D., Zasova L., Loiseau D., Mangold N., Pinet P., Douté S., Schmitt B., Sotin C., Hauber E., Hoffmann H., Jaumann R., Keller U., Arvidson R., Mustard J. F., Duxbury T., Forget F., Neukum G., and the OMEGA Team. 2006. Global mineralogical and aqueous mars history derived from OMEGA/Mars Express data. *Science* 312:400–404. doi:10.1126/science.1122659.

Boctor N., Alexander C. M. O'D., Wang J., and Hauri E. 2003. The sources of water in Martian meteorites: Clues from hydrogen isotopes. *Geochimica et Cosmochimica Acta* 67:3971–3989. doi:10.1016/S0016-7037(03)00234-5.

Boynton W. V., Ming D. W., Kounaves S. P., Young S. M. M., Arvidson R. E., Hecht M. H., Hoffman J., Niles P. B., Hamara D. K., Quinn R. C., Smith P. H., Sutter B., Catling D. C., and Morris R. V. 2009. Evidence for Calcium Carbonate at the Mars Phoenix Landing Site. *Science* 325:61–64. doi:10.1126/science.1172768.

Brearley A. J. 2000. Hydrous phases in ALH 84001: Further evidence for preterrestrial alteration and a shock-induced thermal overprint (abstract #1203). 31st Lunar and Planetary Science Conference. CD-ROM.

Brearley A. J. 2003. Magnetite in ALH 84001: An origin by shock-induced thermal decomposition of iron carbonate. *Meteoritics & Planetary Science* 38:849–870. doi:10.1111/j.1945-5100.2003.tb00283.x.

Bricker O. P., Nesbitt H. W., and Gunter W. D. 1973. Stability of talc. *American Mineralogist* 58:64–72.

Bridges J. C. and Grady M. M. 2000. Evaporite mineral assemblages in the nakhlite (Martian) meteorites. *Earth and Planetary Science Letters* 176:267–279. doi:10.1016/S0012-821X(00)00019-4.

Bridges J. C. and Schwenzer S. P. 2012. The nakhlite hydrothermal brine on Mars. *Earth and Planetary Science Letters* 359:117–123.

Bridges J. C., Catling D. C., Saxton J. M., Swindle T. D., Lyon I. C., and Grady M. M. 2001. Alteration assemblages in martian meteorites: Implications for near-surface processes. In *Chronology and evolution of Mars, Space Sciences Series of ISSI*, edited by Kallenbach R., Geiss J., and Hartmann W. Amsterdam, the Netherlands: Springer. pp. 365–392.

Bridges J. C., Schwenzer S. P., Leveille R., Westall F., Wiens R. C., Mangold N., Bristow T., Edwards P., and Berger G. 2015. Diagenesis and clay mineral formation at Gale Crater, Mars: Gale Crater diagenesis. *Journal of Geophysical Research Planets* 120:1–19. doi:10.1002/2014JE004757.

Cassata W. S., Shuster D. L., Renne P. R., and Weiss B. P. 2012. Trapped Ar isotopes in meteorite ALH 84001 indicate Mars did not have a thick ancient atmosphere. *Icarus* 221:461–465. doi:10.1016/j.icarus.2012.05.005.

Changela H. G. and Bridges J. C. 2010. Alteration assemblages in the nakhlites: Variation with depth on Mars. *Meteoritics & Planetary Science* 45:1847–1867. doi:10.1111/j.1945-5100.2010.01123.x.

Chassefière E. and Leblanc F. 2011a. Constraining methane release due to serpentinization by the observed D/H ratio on Mars. *Earth and Planetary Science Letters* 310:262–271. doi:10.1016/j.epsl.2011.08.013.

Chassefière E. and Leblanc F. 2011b. Methane release and the carbon cycle on Mars. *Planetary and Space Science* 59:207–217. doi:10.1016/j.pss.2010.09.004.

Corrigan C. M. and Harvey R. P. 2004. Multi-generational carbonate assemblages in Martian meteorite Allan Hills 84001: Implications for nucleation, growth, and alteration. *Meteoritics & Planetary Science* 39:17–30. doi:10.1111/j.1945-5100.2004.tb00047.x.

Cudennec Y. and Lecerf A. 2005. Topotactic transformations of goethite and lepidocrocite into hematite and maghemite. *Solid State Sciences* 7:520–529. doi:10.1016/j.solidstatesciences.2005.02.002.

Cudennec Y. and Lecerf A. 2006. The transformation of ferrihydrite into goethite or hematite, revisited. *Journal of Solid State Chemistry* 179:716–722. doi:10.1016/j.jssc.2005.11.030.

Davies P. J. and Bubela B. 1973. The transformation of nesquehonite into hydromagnesite. *Chemical Geology* 12:289–300. doi:10.1016/0009-2541(73)90006-5.

Deit L. L., Hauber E., Fueten F., Pondrelli M., Rossi A. P., and Jaumann R. 2013. Sequence of infilling events in Gale Crater, Mars: Results from morphology, stratigraphy, and mineralogy. *Journal of Geophysical Research Planets* 118:2439–2473. doi:10.1002/2012JE004322.

Dollase W. A. and Reeder R. J. 1986. Crystal structure refinement of huntite, $CaMg_3(CO_3)_4$, with X-ray powder data. *American Mineralogist* 71:163–166.

Ehlmann B. L. and Edwards C. S. 2014. Mineralogy of the Martian Surface. *Annual Review of Earth and Planetary Sciences* 42:291–315. doi:10.1146/annurev-earth-060313-055024.

Ehlmann B. L., Mustard J. F., Murchie S. L., Poulet F., Bishop J. L., Brown A. J., Calvin W. M., Clark R. N., Des Marais D. J., Milliken R. E., Roach L. H., Roush T. L., Swayze G. A., and Wray J. J. 2008. Orbital identification of carbonate-bearing rocks on Mars. *Science* 322:1828–1832. doi:10.1126/science.1164759.

Eiler J. M., Kitchen N., Leshin L., and Strausberg M. 2002a. Hosts of hydrogen in Allan Hills 84001: Evidence for hydrous Martian salts in the oldest Martian meteorite? *Meteoritics & Planetary Science* 37:395–405. doi:10.1111/j.1945-5100.2002.tb00823.x.

Eiler J. M., Valley J. W., Graham C. M., and Fournelle J. 2002b. Two populations of carbonate in ALH84001: Geochemical evidence for discrimination and genesis. *Geochimica et Cosmochimica Acta* 66:1285–1303. doi:10.1016/S0016-7037(01)00847-X.

Fanale F. P., Salvail J. R., Banerdt W. B., and Saunders R. S. 1982. Mars: The regolith-atmosphere-cap system and climate change. *Icarus* 50:381–407. doi:10.1016/0019-1035(82)90131-2.

Farley K. A., Malespin C., Mahaffy P., Grotzinger J. P., Vasconcelos P. M., Milliken R. E., Malin M., Edgett K. S., Pavlov A. A., Hurowitz J. A., Grant J. A., Miller H. B., Arvidson R., Beegle L., Calef F., Conrad P. G., Dietrich W. E., Eigenbrode J., Gellert R., Gupta S., Hamilton V., Hassler D. M., Lewis K. W., McLennan S. M., Ming D., Navarro-González R., Schwenzer S. P., Steele A., Stolper E. M., Sumner D. Y., Vaniman D., Vasavada A., Williford K., Wimmer-Schweingruber R. F., and the MSL Science Team. 2014. In situ radiometric and exposure age dating of the Martian surface. *Science* 343(6169):1247166. doi:10.1126/science.1247166.

Filiberto J. and Schwenzer S. P. 2013. Alteration mineralogy of Home Plate and Columbia Hills—Formation conditions in context to impact, volcanism, and fluvial activity. *Meteoritics & Planetary Science* 48:1937–1957. doi:10.1111/maps.12207.

Fornaca-Rinaldi G., Panichi C., and Tongiorgi E. 1968. Some causes of the variation of the isotopic composition of carbon and oxygen in cave concretions. *Earth and Planetary Science Letters* 4:321–324. doi:10.1016/0012-821X(68)90095-2.

Garrels R. M., Thompson M. E., and Siever R. 1960. Stability of some carbonates at 25 degrees C and one atmosphere total pressure. *American Journal of Science* 258:402–418. doi:10.2475/ajs.258.6.402.

Golden D. C., Ming D. W., Schwandt C. S., Morris R. V., Yang S. V., and Lofgren G. E. 2000. An experimental study on kinetically-driven precipitation of calcium-magnesium-iron carbonates from solution: Implications for the low-temperature formation of carbonates in martian meteorite Allan Hills 84001. *Meteoritics & Planetary Science* 35:457–465. doi:10.1111/j.1945-5100.2000.tb01428.x.

Golden D. C., Ming D. W., Schwandt C. S., Lauer H. V., Socki R. A., Morris R. V., Lofgren G. E., and McKay G. A. 2001. A simple inorganic process for formation of carbonates, magnetite, and sulfides in Martian meteorite ALH84001. *American Mineralogist* 86:370–375.

Golden D. C., Ming D. W., Morris R. V., Brearley A. J., Lauer H. V., Treiman A. H., Zolensky M. E., Schwandt C. S., Lofgren G. E., and McKay G. A. 2004. Evidence for exclusively inorganic formation of magnetite in Martian meteorite ALH 84001. *American Mineralogist* 89:681–695.

Grady M. M., Wright I. P., Douglas C., and Pillinger C. T. 1994. Carbon and nitrogen in ALH84001. *Meteoritics* 29:469.

Greenwood J. P. and McSween H. Y. 2001. Petrogenesis of Allan Hills 84001: Constraints from impact-melted feldspathic and silica glasses. *Meteoritics & Planetary Science* 36:43–62. doi:10.1111/j.1945-5100.2001.tb01809.x.

Greenwood J. P., Mojzsis S. J., and Coath C. D. 2000. Sulfur isotopic compositions of individual sulfides in Martian meteorites ALH 84001 and Nakhla: Implications for crust–regolith exchange on Mars. *Earth and Planetary Science Letters* 184:23–35. doi:10.1016/S0012-821X(00)00301-0.

Grigsby J. D. 2001. Origin and growth mechanism of authigenic chlorite in sandstones of the Lower Vicksburg Formation, South Texas. *Journal of Sedimentary Research* 71:27–36. doi:10.1306/060100710027.

Halevy I., Zuber M. T., and Schrag D. P. 2007. A sulfur dioxide climate feedback on early Mars. *Science* 318:1903–1907. doi:10.1126/science.1147039.

Halevy I., Fischer W. W., and Eiler J. M. 2011. Carbonates in the Martian meteorite Allan Hills 84001 formed at 18 ± 4 °C in a near-surface aqueous environment. *Proceedings of the National Academy of Sciences* 108:16,895–16,899. doi:10.1073/pnas.1109444108.

Hänchen M., Prigiobbe V., Baciocchi R., and Mazzotti M. 2008. Precipitation in the Mg-carbonate system—effects of temperature and $CO_2$ pressure. *Chemical Engineering Science* 63:1012–1028. doi:10.1016/j.ces.2007.09.052.

Harvey R. P. and McSween H. Y. 1996. A possible high-temperature origin for the carbonates in the Martian meteorite ALH84001. *Nature* 382:49–51. doi:10.1038/382049a0.

Hendy C. 1971. The isotopic geochemistry of speleothems—I. The calculation of the effects of different modes of formation on the isotopic composition of speleothems and their applicability as palaeoclimatic indicators. *Geochimica et Cosmochimica Acta* 35:801–824. doi:10.1016/0016-7037(71)90127-X.

Hicks L. J., Bridges J. C., and Gurman S. J. 2014. Ferric saponite and serpentine in the nakhlite martian meteorites. *Geochimica et Cosmochimica Acta* 136:194–210. doi:10.1016/j.gca.2014.04.010.

Hirschmann M. M. and Withers A. C. 2008. Ventilation of $CO_2$ from a reduced mantle and consequences for the early Martian greenhouse. *Earth and Planetary Science Letters* 270:147–155. doi:10.1016/j.epsl.2008.03.034.

Hoefs J. 2009. *Stable isotope geochemistry*, 6th ed. Berlin: Springer.

Holland T. J. B. and Powell R. 2011. An improved and extended internally consistent thermodynamic dataset for phases of petrological interest, involving a new equation of state for solids. *Journal of Metamorphic Geology* 29:333–383. doi:10.1111/j.1525-1314.2010.00923.x.

Holland G., Saxton J. M., Lyon I. C., and Turner G. 2005. Negative δ18O values in Allan Hills 84001 carbonate: Possible evidence for water precipitation on Mars. *Geochimica et Cosmochimica Acta* 69:1359–1370. doi:10.1016/j.gca.2004.08.023.

Hollingbery L. A. and Hull T. R. 2010. The thermal decomposition of huntite and hydromagnesite—A review. *Thermochimica Acta* 509:1–11. doi:10.1016/j.tca.2010.06.012.

Imahashi M. and Takamatsu N. 1976. The dissolution of titanium minerals in hydrochloric and sulfuric acids. *Bulletin of the Chemical Society of Japan* 49:1549–1553. doi:10.1246/bcsj.49.1549.

Jakosky B. M. and Phillips R. J. 2001. Mars' volatile and climate history. *Nature* 412:237–244.

Johnson J. W., Oelkers E. H., and Helgeson H. C. 1992. SUPCRT92: A software package for calculating the standard molal thermodynamic properties of minerals, gases, aqueous species, and reactions from 1 to 5000 bar and 0 to 1000°C. *Computers & Geosciences* 18:899–947. doi:10.1016/0098-3004(92)90029-Q.

Jull A. J. T., Eastoe C. J., and Cloudt S. 1997. Isotopic composition of carbonates in the SNC meteorites, Allan Hills 84001 and Zagami. *Journal of Geophysical Research Planets* 1991–2012(102):1663–1669.

Kinsman D. J. J. 1967. Huntite from a carbonate-evaporite environment. *American Mineralogist* 52:1332.

Kite E. S., Williams J.-P., Lucas A., and Aharonson O. 2014. Low palaeopressure of the Martian atmosphere estimated from the size distribution of ancient craters. *Nature Geoscience* 7:335–339. doi:10.1038/ngeo2137.

Knauth L. P., Brilli M., and Klonowski S. 2003. Isotope geochemistry of caliche developed on basalt. *Geochimica et Cosmochimica Acta* 67:185–195. doi:10.1016/S0016-7037(02)01051-7.

Kopp R. E. and Humayun M. 2003. Kinetic model of carbonate dissolution in Martian meteorite ALH 84001. *Geochimica et Cosmochimica Acta* 67:3247–3256. doi:10.1016/S0016-7037(02)01114-6.

Kring D., Swindle T., Gleason J., and Grier J. 1998. Formation and relative ages of maskelynite and carbonate in ALH 84001. *Geochimica et Cosmochimica Acta* 62:2155–2166. doi:10.1016/S0016-7037(98)00133-1.

Lapen T. J., Righter M., Brandon A. D., Debaille V., Beard B. L., Shafer J. T., and Peslier A. H. 2010. A younger age for ALH 84001 and its geochemical link to shergottite sources in Mars. *Science* 328:347–351. doi:10.1126/science.1185395.

Leshin L. A., Epstein S., and Stolper E. M. 1996. Hydrogen isotope geochemistry of SNC meteorites. *Geochimica et Cosmochimica Acta* 60:2635–2650. doi:10.1016/0016-7037(96)00122-6.

Leshin L. A., McKeegan K. D., Carpenter P. K., and Harvey R. P. 1998. Oxygen isotopic constraints on the genesis of carbonates from Martian meteorite ALH 84001. *Geochimica et Cosmochimica Acta* 62:3–13. doi:10.1016/S0016-7037(97)00331-1.

Lodders K. 1998. A survey of shergottite, nakhlite and chassigny meteorites whole-rock compositions. *Meteoritics & Planetary Science* 33:A183–A190. doi:10.1111/j.1945-5100.1998.tb01331.x.

Ludvigson G. A., González L. A., Fowle D. A., Roberts J. A., Driese S. G., Villarreal M. A., Smith J. J., and Suarez M. B. 2013. Paleoclimatic applications and modern process studies of pedogenic siderite. New frontiers in paleopedology and terrestrial paleoclimatology. *Society of Economic Paleontologists and Mineralogists Special Publication* 104:79–87. doi:10.2110/sepmsp.104.01.

Mahaffy P. R., Webster C. R., Atreya S. K., Franz H., Wong M., Conrad P. G., Harpold D., Jones J. J., Leshin L. A., Manning H., Owen T., Pepin R. O., Squyres S., Trainer M., and MSL Science Team. 2013. Abundance and isotopic composition of gases in the Martian atmosphere from the Curiosity rover. *Science* 341:263–266. doi:10.1126/science.1237966.

McCollom T. M. 2013. Laboratory simulations of abiotic hydrocarbon formation in Earth's deep subsurface. *Reviews in Mineralogy and Geochemistry* 75:467–494. doi:10.2138/rmg.2013.75.15.

McKay D. S., Gibson E. K., Thomas-Keprta K. L., Vali H., Romanek C. S., Clemett S. J., Chillier X. D. F., Maechling C. R., and Zare R. N. 1996. Search for past life on Mars: Possible relic biogenic activity in Martian meteorite ALH 84001. *Science* 273:924–930.

McSween H. Y. and Harvey R. P. 1998. An evaporation model for formation of carbonates in the ALH 84001 Martian meteorite. *International Geologiy Review* 40:774–783. doi:10.1080/00206819809465238.

Ming D. W., Archer P. D., Glavin D. P., Eigenbrode J. L., Franz H. B., Sutter B., Brunner A. E., Stern J. C., Freissinet C., McAdam A. C., Mahaffy P. R., Cabane M., Coll P., Campbell J. L., Atreya S. K., Niles P. B., Bell J. F., Bish D. L., Brinckerhoff W. B., Buch A., Conrad P. G., Des Marais D. J., Ehlmann B. L., Fairén A. G., Farley K., Flesch G. J., Francois P., Gellert R., Grant J. A., Grotzinger J. P., Gupta S., Herkenhoff K. E., Hurowitz J. A., Leshin L. A., Lewis K. W., McLennan S. M., Miller K. E., Moersch J., Morris R. V., Navarro-González R., Pavlov A. A., Perrett G. M., Pradler I., Squyres S. W., Summons R. E., Steele A., Stolper E. M., Sumner D. Y., Szopa C., Teinturier S., Trainer M. G., Treiman A. H., Vaniman D. T., Vasavada A. R., Webster C. R., Wray J. J., Yingst R. A., and MSL Science Team. 2014. Volatile and organic compositions of sedimentary rocks in Yellowknife Bay, Gale Crater, Mars. *Science* 343(6169):1245267. doi:10.1126/science.1245267.

Mittlefehldt D. W. 1994. ALH 84001, a cumulate orthopyroxenite member of the Martian meteorite clan. *Meteoritics* 29:214–221.

Morris R. V., Ruff S. W., Gellert R., Ming D. W., Arvidson R. E., Clark B. C., Golden D. C., Siebach K., Klingelhöfer G., Schröder C., Fleischer I., Yen A. S., and Squyres S. W. 2010. Identification of carbonate-rich outcrops on Mars by the Spirit rover. *Science* 329:421–424. doi:10.1126/science.1189667.

Mustard J. F., Murchie S. L., Pelkey S. M., Ehlmann B. L., Milliken R. E., Grant J. A., Bibring J.-P., Poulet F., Bishop J., Dobrea E. N., Roach L., Seelos F., Arvidson R. E., Wiseman S., Green R., Hash C., Humm D., Malaret E., McGovern J. A., Seelos K., Clancy T., Clark R., Marais D. D., Izenberg N., Knudson A., Langevin Y., Martin T., McGuire P., Morris R., Robinson M., Roush T., Smith M., Swayze G., Taylor H., Titus T., and Wolff M. 2008. Hydrated silicate minerals on Mars observed by the Mars Reconnaissance Orbiter CRISM instrument. *Nature* 454:305–309. doi:10.1038/nature07097.

Niles P. B., Leshin L. A., and Guan Y. 2005. Microscale carbon isotope variability in ALH 84001 carbonates and a discussion of possible formation environments. *Geochimica et Cosmochimica Acta* 69:2931–2944. doi:10.1016/j.gca.2004.12.012.

Niles P. B., Zolotov M. Y., and Leshin L. A. 2009. Insights into the formation of Fe- and Mg-rich aqueous solutions on early Mars provided by the ALH 84001 carbonates. *Earth and Planetary Science Letters* 286:122–130. doi:10.1016/j.epsl.2009.06.039.

Niles P., Catling D., Berger G., Chassefière E., Ehlmann B., Michalski J., Morris R., Ruff S., and Sutter B. 2013. Geochemistry of carbonates on Mars: Implications for climate history and nature of aqueous environments. *Space Science Reviews* 174:301–328. doi:10.1007/s11214-012-9940-y.

Nyquist L. E., Bogard D. D., Shih C. Y., Greshake A., Stöffler D., and Eugster O. 2001. Ages and geologic histories of Martian meteorites. *Space Science Reviews* 96:105–164.

Owen T., Biemann K., Rushneck D. R., Biller J. E., Howarth D. W., and Lafleur A. L. 1977. The composition of the atmosphere at the surface of Mars. *Journal of Geophysical Research* 82:4635–4639. doi:10.1029/JS082i028p04635.

Pollack J. B., Kasting J. F., Richardson S. M., and Poliakoff K. 1987. The case for a wet, warm climate on early Mars. *Icarus* 71:203–224. doi:10.1016/0019-1035(87)90147-3.

Ramirez R. M., Kopparapu R., Zugger M. E., Robinson T. D., Freedman R., and Kasting J. F. 2014. Warming early Mars with $CO^2$ and $H^2$. *Nature Geoscience* 7:59–63.

Reed M. H. 1982. Calculation of multicomponent chemical equilibria and reaction processes in systems involving minerals, gases and an aqueous phase. *Geochimica et Cosmochimica Acta* 46:513–528. doi:10.1016/0016-7037(82)90155-7.

Reed M. H. 1998. Calculation of simultaneous chemical equilibria in aqueous-mineral-gas systems and its application to modeling hydrothermal processes. In *Techniques in hydrothermal ore deposits geology*, edited by Richards J. P. and Larson P. B. Reviews in Economic Geology. 10:109–124.

Retallack G. J. 2014. Paleosols and paleoenvironments of early Mars. *Geology* 42:755–758. doi:10.1130/G35912.1.

Richard F. C. and Bourg A. C. M. 1991. Aqueous geochemistry of chromium: A review. *Water Research* 25:807–816. doi:10.1016/0043-1354(91)90160-R.

Romanek C. S., Grady M. M., Wright I. P., Mittlefehldt D. W., Socki R. A., Pillinger C. T., and Gibson E. K. 1994. Record of fluid-rock interactions on Mars from the meteorite ALH 84001. *Nature* 372:655–657. doi:10.1038/372655a0.

Ruff S. W., Niles P. B., Alfano F., and Clarke A. B. 2014. Evidence for a Noachian-aged ephemeral lake in Gusev crater, Mars. *Geology* 42:359–362. doi:10.1130/G35508.1.

Saldi G. D., Jordan G., Schott J., and Oelkers E. H. 2009. Magnesite growth rates as a function of temperature and saturation state. *Geochimica et Cosmochimica Acta* 73:5646–5657. doi:10.1016/j.gca.2009.06.035.

Schwenzer S. P., Bridges J. C., Wiens R. C., Conrad P. G., Kelley S. P., Leveille R., Mangold N., Martin-Torres J., McAdam A., Newsom H., Zorzano M. P., Rapin W., Spray J., Treiman A. H., Westall F., Fairén A. G., and Meslin P.-Y. 2016. Fluids during diagenesis and sulfate vein formation in sediments at Gale Crater, Mars. *Meteoritics & Planetary Science* (this volume). doi 10.1111/maps.12668.

Schwenzer S. P. and Kring D. A. 2009. Impact-generated hydrothermal systems capable of forming phyllosilicates on Noachian Mars. *Geology* 37:1091–1094. doi:10.1130/G30340A.1.

Schwenzer S. P. and Kring D. A. 2013. Alteration minerals in impact-generated hydrothermal systems—Exploring host rock variability. *Icarus* 226:487–496. doi:10.1016/j.icarus.2013.06.003.

Schwertmann U. and Murad E. 1983. Effect of pH on the formation of goethite and hematite from ferrihydrite. *Clays and Clay Minerals* 31:277–284.

Scott E. R. D. 1999. Origin of carbonate-magnetite-sulfide assemblages in Martian meteorite ALH 84001. *Journal of Geophysical Research* 104:3803. doi:10.1029/1998JE900034.

Scott E. R. D., Yamaguchi A., and Krot A. N. 1997. Petrological evidence for shock melting of carbonates in the Martian meteorite ALH 84001. *Nature* 387:377–379. doi:10.1038/387377a0.

Seewald J. S., Zolotov M. Y., and McCollom T. 2006. Experimental investigation of single carbon compounds under hydrothermal conditions. *Geochimica et Cosmochimica Acta* 70:446–460. doi:10.1016/j.gca.2005.09.002.

Shearer C. K., Leshin L. A., and Adcock C. T. 1999. Olivine in Martian meteorite ALH 84001: Evidence for a high-temperature origin and implications for signs of life. *Meteoritics & Planetary Science* 34:331–339. doi:10.1111/j.1945-5100.1999.tb01343.x.

Sheppard S. F. and Schwarcz H. 1970. Fractionation of carbon and oxygen isotopes and magnesium between coexisting metamorphic calcite and dolomite. *Contributions to Mineralogy and Petrology* 26:161–198. doi:10.1007/BF00373200.

Sofer Z. and Gat J. R. 1975. The isotope composition of evaporating brines: Effect of the isotopic activity ratio in saline solutions. *Earth and Planetary Science Letters* 26:179–186. doi:10.1016/0012-821X(75)90085-0.

Spycher N. F. and Reed M. H. 1988. Fugacity coefficients of $H_2$, $CO_2$, $CH_4$, $H_2O$ and of $H_2O$- $CO_2$-$CH_4$ mixtures: A virial equation treatment for moderate pressures and temperatures applicable to calculations of hydrothermal boiling. *Geochimica et Cosmochimica Acta* 52:739–749. doi:10.1016/0016-7037(88)90334-1.

Stanger G. and Neal C. 1994. The occurrence and chemistry of huntite from Oman. *Chemical Geology* 112:247–254. doi:10.1016/0009-2541(94)90027-2.

Steele A., Fries M. D., Amundsen H. E. F., Mysen B. O., Fogel M. L., Schweizer M., and Boctor N. Z. 2007. Comprehensive imaging and Raman spectroscopy of carbonate globules from Martian meteorite ALH 84001 and a terrestrial analogue from Svalbard. *Meteoritics & Planetary Science* 42:1549–1566. doi:10.1111/j.1945-5100.2007.tb00590.x.

Steele A., McCubbin F. M., Fries M., Kater L., Boctor N. Z., Fogel M. L., Conrad P. G., Glamoclija M., Spencer M., Morrow A. L., Hammond M. R., Zare R. N., Vicenzi E. P., Siljeström S., Bowden R., Herd C. D. K., Mysen B. O., Shirey S. B., Amundsen H. E. F., Treiman A. H., Bullock E. S., and Jull A. J. T. 2012a. A reduced organic carbon component in Martian basalts. *Science* 337:212–215. doi:10.1126/science.1220715.

Steele A., McCubbin F. M., Fries M. D., Golden D. C., Ming D. W., and Benning L. G. 2012b. Graphite in the Martian meteorite Allan Hills 84001. *American Mineralogist* 97:1256–1259.

Sugiura N. and Hoshino H. 2000. Hydrogen-isotopic compositions in Allan Hills 84001 and the evolution of the martian atmosphere. *Meteoritics & Planetary Science* 35:373–380. doi:10.1111/j.1945-5100.2000.tb01783.x.

Tanger J. C. and Helgeson H. C. 1988. Calculation of the thermodynamic and transport properties of aqueous species at high pressures and temperatures; revised equations of state for the standard partial molal properties of ions and electrolytes. *American Journal of Science* 288:19–98. doi:10.2475/ajs.288.1.19.

Thomas-Keprta K. L., Bazylinski D. A., Kirschvink J. L., Clemett S. J., McKay D. S., Wentworth S. J., Vali H., Gibson E. K. Jr., and Romanek C. S. 2000. Elongated prismatic magnetite crystals in ALH 84001 carbonate globules: Potential Martian magnetofossils. *Geochimica et Cosmochimica Acta* 64:4049–4081. doi:10.1016/S0016-7037(00)00481-6.

Thomas-Keprta K. L., Clemett S. J., McKay D. S., Gibson E. K., and Wentworth S. J. 2009. Origins of magnetite nanocrystals in Martian meteorite ALH 84001. *Geochimica et Cosmochimica Acta* 73:6631–6677. doi:10.1016/j.gca.2009.05.064.

Thomson B. J., Bridges N. T., Milliken R., Baldridge A., Hook S. J., Crowley J. K., Marion G. M., de Souza Filho C. R., Brown A. J., and Weitz C. M. 2011. Constraints on the origin and evolution of the layered mound in Gale Crater, Mars using Mars Reconnaissance Orbiter data. *Icarus* 214:413–432. doi:10.1016/j.icarus.2011.05.002.

Tosca N. J., Macdonald F. A., Strauss J. V., Johnston D. T., and Knoll A. H. 2011. Sedimentary talc in Neoproterozoic carbonate successions. *Earth and Planetary Science Letters* 306:11–22. doi:10.1016/j.epsl.2011.03.041.

Treiman A. H. 1995. A petrographic history of Martian meteorite ALH 84001: Two shocks and an ancient age. *Meteoritics* 30:294.

Treiman A. H. 1997. Chemical disequilibrium in carbonate minerals of Martian meteorite ALH 84001—Inconsistent with high formation temperature (abstract #1445). 28th Lunar and Planetary Science Conference. CD-ROM.

Treiman A. H. 1998. The history of Allan Hills 84001 revised: Multiple shock events. *Meteoritics & Planetary Science* 33:753–764. doi:10.1111/j.1945-5100.1998.tb01681.x.

Treiman A. H. 2003. Submicron magnetite grains and carbon compounds in Martian meteorite ALH 84001: Inorganic, abiotic formation by shock and thermal metamorphism. *Astrobiology* 3:369–392. doi:10.1089/153110703769016451.

Treiman A. H. 2005. Olivine and carbonate globules in ALH84001: A terrestrial analog, and implications for water on Mars (abstract #1107). 36th Lunar and Planetary Science Conference. CD-ROM.

Treiman A. H. and Essene E. J. 2011. Chemical composition of magnetite in Martian meteorite ALH 84001: Revised appraisal from thermochemistry of phases in Fe–Mg–C–O. *Geochimica et Cosmochimica Acta* 75:5324–5335. doi:10.1016/j.gca.2011.06.038.

Treiman A. H. and Romanek C. S. 1998. Bulk and stable isotopic compositions of carbonate minerals in Martian meteorite Allan Hills 84001: No proof of high formation temperature. *Meteoritics & Planetary Science* 33:737–742. doi:10.1111/j.1945-5100.1998.tb01679.x.

Treiman A. H., Amundsen H. E., Blake D. F., and Bunch T. 2002. Hydrothermal origin for carbonate globules in Martian meteorite ALH 84001: A terrestrial analogue from Spitsbergen (Norway). *Earth and Planetary Science Letters* 204:323–332. doi:10.1016/S0012-821X(02)00998-6.

Valley J. W., Eiler J. M., Graham C. M., Gibson E. K., Romanek C. S., and Stolper E. M. 1997. Low-temperature carbonate concretions in the Martian meteorite ALH84001: Evidence from stable isotopes and mineralogy. *Science* 275:1633–1638. doi:10.1126/science.275.5306.1633.

Van Berk W. and Fu Y. 2011. Reproducing hydrogeochemical conditions triggering the formation of carbonate and phyllosilicate alteration mineral assemblages on Mars (Nili Fossae region). *Journal of Geophysical Research* 116: doi:10.1029/2011JE003886.

Van Berk W., Ilger J.-M., Fu Y., and Hansen C. 2011. Decreasing $CO_2$ partial pressure triggered Mg–Fe–Ca carbonate formation in ancient Martian crust preserved in the ALH 84001 Meteorite. *Geofluids* 11:6–17. doi:10.1111/j.1468-8123.2010.00296.x.

Van Berk W., Fu Y., and Ilger J.-M. 2012. Reproducing early Martian atmospheric carbon dioxide partial pressure by modeling the formation of Mg-Fe-Ca carbonate identified in the Comanche rock outcrops on Mars. *Journal of Geophysical Research* 117: doi:10.1029/2012JE004173.

Vaniman D. T., Bish D. L., Ming D. W., Bristow T. F., Morris R. V., Blake D. F., Chipera S. J., Morrison S. M., Treiman A. H., Rampe E. B., Rice M., Achilles C. N., Grotzinger J. P., McLennan S. M., Williams J., Bell J. F., Newsom H. E., Downs R. T., Maurice S., Sarrazin P., Yen A. S., Morookian J. M., Farmer J. D., Stack K., Milliken R. E., Ehlmann B. L., Sumner D. Y., Berger G., Crisp J. A., Hurowitz J. A., Anderson R., Des Marais D. J., Stolper E. M., Edgett K. S., Gupta S., Spanovich N., and the MSL Science Team. 2014. Mineralogy of a mudstone at Yellowknife Bay, Gale Crater, Mars. *Science* 343(6169):1243480. doi:10.1126/science.1243480.

Velbel M. A., Long D. T., and Gooding J. L. 1991. Terrestrial weathering of Antarctic stone meteorites: Formation of Mg-carbonates on ordinary chondrites. *Geochimica et Cosmochimica Acta* 55:67–76. doi:10.1016/0016-7037(91)90400-Y.

Warren P. H. 1998. Petrologic evidence for low-temperature, possibly flood evaporitic origin of carbonates in the ALH 84001 meteorite. *Journal of Geophysical Research Planets* 103:16,759–16,773. doi:10.1029/98JE01544.

Webster C. R., Mahaffy P. R., Atreya S. K., Flesch G. J., Mischna M. A., Meslin P.-Y., Farley K. A., Conrad P. G., Christensen L. E., Pavlov A. A., Martín-Torres J., Zorzano M.-P., McConnochie T. H., Owen T., Eigenbrode J. L., Glavin D. P., Steele A., Malespin C. A., Archer P. D., Sutter B., Coll P., Freissinet C., McKay C. P., Moores J. E., Schwenzer S. P., Bridges J. C., Navarro-Gonzalez R., Gellert R., Lemmon M. T., and the MS Team. 2015. Mars methane detection and variability at Gale crater. *Science* 347:415–417.

Wordsworth R., Forget F., Millour E., Head J. W., Madeleine J.-B., and Charnay B. 2013. Global modelling of the early Martian climate under a denser $CO_2$ atmosphere: Water cycle and ice evolution. *Icarus* 222:1–19. doi:10.1016/j.icarus.2012.09.036.

Wray J. J., Murchie S. L., Bishop J. L., Ehlmann B. L., Milliken R. E., Wilhelm M. B., Seelos K. D., and Chojnacki M. 2016. Orbital evidence for more widespread carbonate-bearing rocks on Mars: More widespread carbonate rocks on Mars. *Journal of Geophysical Research Planets* 121:652–677. doi:10.1002/2015JE004972.

Zolensky M. E., Bourcier W. L., and Gooding J. L. 1988. Computer modeling of the mineralogy of the Martian surface, as modified by aqueous alteration. In *Workshop on Mars sample return science*, edited by Drake M. J. Greeley R., McKay G. A., Blanchard D. P., Carr M. H., Gooding J. L., McKay C. P., Spudis P. D. and Squyres S. W. Houston, TX: Lunar and Planetary Institute. pp. 188–189.

Zolotov M. and Shock E. 1999. Abiotic synthesis of polycyclic aromatic hydrocarbons on Mars. *Journal of Geophysical Research Planets* 104:14,033–14,049. doi:10.1029/1998JE000627.

## SUPPORTING INFORMATION

Additional supporting information may be found in the online version of this article:

**Fig. S1:** Formation temperatures of the carbonates in ALH 84001, from literature.

**Fig S2:** Saturation indices (log10 (Q/K)) of the carbonate minerals in the models.

**Table S1:** Minerals disallowed from forming in the models.

**Table S2:** All minerals formed in the models, their mineral groups, and chemical formula.